

Deposition, diagenetic and hydrothermal processes in the Aptian Pre-Salt lacustrine carbonate reservoirs of the northern Campos Basin, offshore Brazil



Bruno Eustáquio Moreira Lima ^{a,b,*}, Luiz Fernando De Ros ^{b,***}

^a Petrobras S.A., Av. República do Chile 330, 24th floor, East Tower, Rio de Janeiro, RJ 20031-170, Brazil

^b Geosciences Institute, Rio Grande do Sul Federal University, Av. Bento Gonçalves 9500, Porto Alegre, RS 91509-900, Brazil

ARTICLE INFO

Article history:

Received 31 October 2018

Received in revised form 16 January 2019

Accepted 19 January 2019

Available online 4 February 2019

Editor: C. Chague

Keywords:

Pre-Salt
Lacustrine carbonates
Campos Basin
Hydrothermal fluids
Dolomitization
Silicification

ABSTRACT

The discovery of large oil accumulations in the rift and sag Pre-Salt sections of the Campos and Santos Basins has revived interest in the exploration of the lacustrine carbonate reservoirs in the Brazilian and African marginal basins. More than half of Brazilian oil production originates from the Pre-Salt reservoirs of these offshore basins. A study integrating systematic petrography, cathodoluminescence, scanning electron microscopy, microprobe and X-ray diffraction was performed on seven wells in the northern Campos Basin. This study highlights the major primary, diagenetic and hydrothermal features of the Pre-Salt succession, with the aim to improve our understanding of the factors that influence the porosity and permeability distribution in these important lacustrine carbonate reservoirs. The Pre-Salt deposits correspond to bioclastic grainstones and rudstones, syngenetic crusts of fascicular calcite, and intraclastic grainstones and rudstones of reworked crust fragments and calcite spherulites. Magnesian silicates are frequently associated with carbonate deposits. In the sag phase, stevensitic laminations constitute the substrate for the precipitation of calcite crusts and spherulites, which displace and replace the syngenetic magnesian clay deposits. In the rift section, stevensitic ooids are mixed with bioclasts or form ooidal arenites. Pre-Salt carbonate reservoirs have undergone a complex and heterogeneous diagenetic evolution. Eodiagenetic processes include the dissolution, neomorphism and cementation of bivalve bioclasts in the rift, as well as the dissolution of magnesian silicates and their replacement by calcite spherulites, silica and dolomite in the sag section. Burial alterations are commonly associated with hydrothermal fluids carried through faults and fracture systems. These fluids promote dolomitization, silicification, and dissolution at varying degrees and intensities. Eodiagenetic precipitation and dissolution owing to variations in the lake water chemistry and the episodic flow of hydrothermal fluids under burial conditions control the creation, redistribution, and obliteration of porosity in the Pre-Salt reservoirs.

© 2019 Elsevier B.V. All rights reserved.

1. Introduction

In recent years, huge hydrocarbon reserves have been discovered in the so-called Pre-Salt lacustrine carbonate reservoirs along the South Atlantic conjugate margins, mainly in the Campos and Santos Basins of Brazil (Carminatti et al., 2009) and in the Kwanza Basin of Angola (Saller et al., 2016). Thus, an increasing number of wells are being drilled in this prolific oil province, which provide new data and progressive detail of the complex character of the depositional processes and diagenetic alteration of the Pre-Salt deposits. In several Pre-Salt fields, diagenetic processes have directly altered and/or reorganized the

porosity architecture of the carbonate fabric, consequently affecting the porosity and permeability characteristics of the reservoir rocks.

Pre-Salt reservoirs from the northern Campos Basin occur in the Lower Cretaceous carbonate deposits of the Coqueiros and Macabu Formations (Dias et al., 1988; Winter et al., 2007). The Coqueiros Formation reservoirs correspond to the bioclastic deposits of bivalves, known as “coquinas” (Baumgarten et al., 1988; Dias et al., 1988; Muniz and Bosence, 2015). The Macabu Formation contains intervals of fascicular calcite and spherulitic aggregates interspersed with intraclastic deposits that have been reworked from these precipitates and laminated strata made of syngenetic magnesian clay minerals and siliciclastic mud (e.g., Tosca and Wright, 2014; Wright and Barnett, 2015; Wright and Tosca, 2016; Herlinger Jr. et al., 2017).

Wright and Barnett (2015) proposed that the characteristic deposition of the Aptian Pre-Salt succession is arranged in cyclothsems composed of laminated sediments of syngenetic magnesian clays at the base, syngenetic magnesian deposits partially replaced and

* Correspondence to: B.E.M. Lima, Petrobras S.A., Av. República do Chile 330, 24th floor, East Tower, Rio de Janeiro, RJ 20031-170, Brazil.

** Corresponding author.

E-mail addresses: brunolima@petrobras.com.br (B.E.M. Lima), lfderos@inf.ufrgs.br (L.F. De Ros).

displaced by calcite spherulites in the middle, and fascicular calcite crusts at the top. According to those authors, the alternation of calcite or stevensite precipitation in these deposits was related to variations in the pH, Mg and Ca activity, temperature, and pCO_2 in the geochemistry of lacustrine waters. Wright and Tosca (2016) presented an evaporitic geochemical model to explain the unusual calcite morphologies observed in these cyclothsems. Alternatively, the spherulites were interpreted as ooid-like particles formed by nucleation on the sediment–water interface under the influence of organic constituents (e.g., Mercedes-Martín et al., 2016, 2017; Chafetz et al., 2018).

The intense and heterogeneous diagenesis of the Pre-Salt deposits resulted in large vertical and lateral variations in the quality (permeability and porosity) of the reservoirs. Although depositional features exerted significant control over the diagenetic processes, most of the porosity that is currently present in the Pre-Salt reservoirs is of secondary origin (Tosca and Wright, 2015). Dolomitization, silicification, cementation, dissolution, and/or recrystallization were promoted in association with tectonic and hydraulic fracturing (Herlinger Jr. et al., 2017; Poros et al., 2017; Vieira de Luca et al., 2017). It is interpreted that these alterations may have been related to processes occurring during burial and to the flow of hydrothermal fluids. Recently, many authors have pointed out compelling evidence of hydrothermal activity in the Campos (e.g., Alvarenga et al., 2016; Lepley et al., 2017; Vieira de Luca et al., 2017) and Kwanza Basins (e.g., Teboul et al., 2017, 2019), associated mainly with magmatic events.

The hydrothermal alteration of carbonate deposits has recently been the subject of extensive debate by the scientific community (e.g., Machel and Lonnee, 2002; Davies, 2004; Machel, 2004; Davies and Smith, 2006). In general, the hydrothermal alteration of carbonate sequences involves the action of complex physicochemical processes on pre-existing rocks, which is related to interactions with hot fluids promoting the precipitation of “unusual” cements, including saddle dolomite, fluorite, barite, anhydrite, sphalerite, and pyrite (Neilson and Oxtoby, 2008). Hydrothermal processes are evidence for a local geothermal anomaly and require a mechanism or conduit that allows fluid flow, such as deep-buried fault systems.

The silicification of carbonate sediments can apparently occur at different stages of their diagenetic evolution. Examples of eodiagenetic and mesodiagenetic silicification have been described in the literature (e.g., Hesse, 1989). Packard et al. (2001) reported carbonate reservoirs modified by dolomitization, silicification, and dissolution related to the percolation of hydrothermal fluids. Vieira de Luca et al. (2017) and Poros et al. (2017) suggested that the percolation of hydrothermal fluids promoted extensive silicification in the Pre-Salt reservoirs of the Campos and Kwanza Basins, respectively.

The objective of this study is to characterize and interpret the depositional, diagenetic and hydrothermal conditions under which the Pre-Salt reservoirs from the northern Campos Basin were generated and modified. This study will contribute to the development of more realistic reservoir models. Specific aims involve the characterization of processes and products of probable hydrothermal circulation throughout faults and fractures, as well as their impact on the porosity, permeability and heterogeneity of the reservoirs.

2. Geological context

The Campos Basin is located on the southeastern Brazilian margin, approximately between the 21st and 23rd south parallels (Fig. 1). It covers a total area of approximately 100,000 km², with only 5800 km² onshore. The study area is located in the northern Campos Basin (Fig. 1) in deep to ultra-deep waters. The basin originated from rifting of the Gondwana Continent during the Neocomian (lowermost Cretaceous), which eventually formed the South Atlantic Ocean through separation of the American and African continents (e.g., Rabinowitz and LaBrecque, 1979; Austin and Uchupi, 1982; Nürnberg and Müller, 1991; Cainelli and Mohriak, 1999). It is aligned with the Kwanza Basin on the

African side. Winter et al. (2007) divided the tectono-stratigraphic evolution of the Campos Basin into rift, post-rift, and drift supersequences.

The rift supersequence was generated during the initial evolution of the basin and is represented by both the volcanic Cabiúnas Formation and the basal interval of the Lagoa Feia Group, which corresponds to the Itabapoana, Atafona, and Coqueiros Formations, deposited from the Barremian to the Lower Aptian (Fig. 2). According to McKenzie (1978) and White and McKenzie (1988), the rift phase of the basin, which extended from the Hauterivian to the Aptian, was determined by the extension of the lithosphere and by the asthenospheric elevation, related to widespread intracratonic tholeiitic volcanism (Turner et al., 1994; Mohriak et al., 2008; Torsvik et al., 2009). The basal, rift section portion of the Lagoa Feia Group, is limited at the top by the so-called Pre-Alagoas regional unconformity. The Itabapoana Formation is composed of proximal marginal sediments, including conglomerates, sandstones, siltstones, and red shales, whereas the Atafona Formation mostly comprises arenites and siltstones constituted by ooids of stevensite, kerolite and other syngenetic magnesian layer silicates that accumulated in alkaline lakes (Bertani and Carozzi, 1985a, 1985b; Dias et al., 1988; Abrahão and Warme, 1990).

The Coqueiros Formation consists of mainly carbonate rudstones and grainstones of ostracod, gastropod and mostly bivalve bioclasts intercalated with organic shales (e.g., Baumgarten et al., 1988; Dias et al., 1988; Thompson et al., 2015). Models proposed for the depositional environment of these rift bioclastic deposits have related these deposits to playa-lake and pluvial-lake environments (Bertani and Carozzi, 1985a); storm events, bioaccumulated banks, and deep lacustrine environments (Carvalho et al., 2000); and gravitational re-deposition from shallow to deeper lacustrine settings (Goldberg et al., 2017).

The post-rift supersequence, which contains the upper interval of the Lagoa Feia Group, was deposited on the regional Pre-Alagoas unconformity during the so-called sag stage of the basin. This supersequence comprises the Itabapoana, Gargaú, Macabu, and Retiro Formations that were deposited during the Middle/Upper Aptian (Fig. 2). The Gargaú Formation comprises sandstones, mudrocks, and carbonates deposited in a lacustrine environment, which grade laterally to the proximal clastic sediments of the Itabapoana Formation (Winter et al., 2007).

The Macabu Formation was deposited in alkaline lacustrine environments under arid climate conditions and comprises argillaceous and carbonate laminites, spherulitic carbonate deposits and crusts, which were originally interpreted as microbial stromatolites (Dias, 2005; Muniz and Bosence, 2015). These deposits have been re-interpreted as chemical precipitates controlled by the geochemistry of lacustrine waters (e.g., Tosca and Wright, 2014; Wright and Barnett, 2014, 2015; Wright and Tosca, 2016). A hybrid biotic/abiotic precipitation probably occurs in the Pre-Salt deposits. However, the abiotic chemical is the dominant control in the precipitation of the majority of the constituents, as evidenced by features that were observed in the petrographic study.

The upper portion of the post-rift supersequence corresponds to the Retiro Formation (Fig. 2), which is a thick accumulation of evaporites (Upper Alagoas). This sequence was deposited during the advent of marine incursions under arid climate conditions (Leyden et al., 1976; Winter et al., 2007) and consists essentially of anhydrite, halite, sylvite, and carnallite. These evaporites provide a stratigraphic seal for the large hydrocarbon accumulations of the Pre-Salt petroleum province.

3. Materials and methods

For this study, samples from seven wells, comprising four cores, 358 core plugs and 199 sidewall core samples were taken from pervasively dolomitized and silicified portions of the Pre-Salt interval. Standard-thickness thin sections were prepared from 289 blue epoxy resin-impregnated samples for transmitted light microscopy. Staining with Alizarin red-S and potassium ferricyanide solution was applied to all

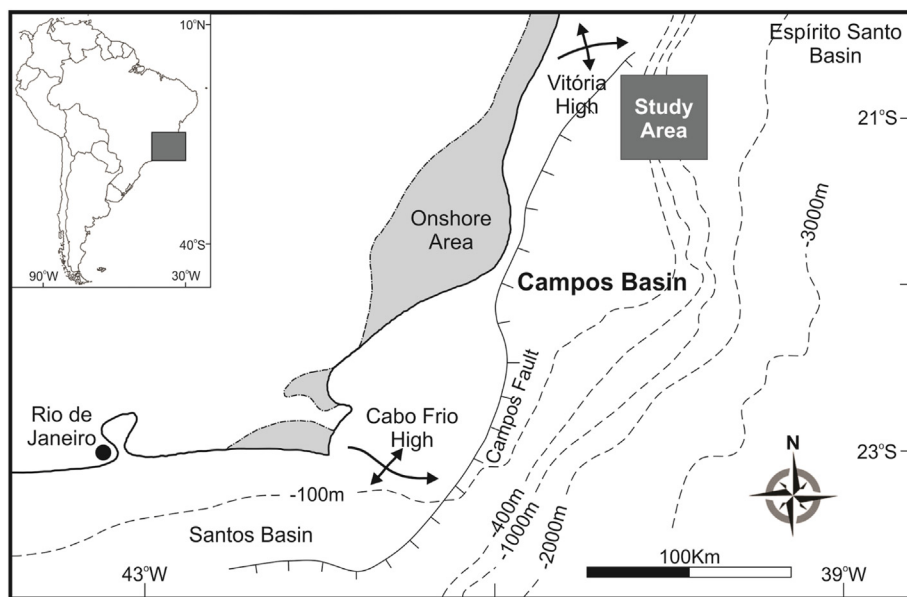


Fig. 1. Map showing major structural features of Campos Basin and the location of study area (modified from Dias et al., 1988).

thin sections to differentiate the carbonate minerals as outlined by Dickson (1965). Pore types were classified according to Choquette and Pray (1970). All thin sections were examined in petrographic microscopes between uncrossed (//P) and crossed polarizers (XP). Quantitative petrography was performed on 88 representative thin sections using the Petroledge® software version Workstation 3.4.18.1111 by counting 300 points per sample to evaluate the porosity and the primary detrital, syngenetic, and diagenetic constituents of the samples. Cathodoluminescence (CL) microscopy was conducted on 13 polished thin sections using a hot cathode apparatus mounted on a Zeiss Axiocam MRC polarizing microscope.

Scanning electron microscopy with secondary electrons (SEM) and with backscattered electrons (BSE) with the support of energy-dispersive spectrometry (EDS) was performed at the Regional Center for Technological Development and Innovation (CRTI) of the Federal University of Goiás (UFG). For BSE examination, twelve polished thin sections were coated with carbon in a JEOL-JEE-420 vacuum evaporator. SEM investigation of five samples by backscattered and secondary electrons, was conducted using a JSM-IT300 JEOL electron microscope. Energy-dispersed spectroscopy (EDS) was performed using an OXFORD X-MaxN X-ray detector equipment with the aim of recognizing the

elemental mineral composition in rock fragments and thin sections. Wavelength-dispersive X-ray spectroscopy (WDS) was conducted for quantitative elemental analysis on nine polished and carbon-coated thin sections, using a JEOL JXA-8230 electron microprobe with five WDS detectors. In addition, twenty thin sections were selected for automated mineralogical distribution mapping using QEMSCAN 650 (FEI) equipment with two coupled EDS/Bruker detectors.

X-ray diffraction (XRD) quantitative analyses were obtained from 453 samples (Supplementary material) for the identification of the total composition, clay minerals and other constituents in the fine fraction (<2 µm). Mechanical methods were used to fragment the carbonate samples, while avoiding milling so as not to modify the crystalline structure of the clay minerals. Subsequently, some sample centrifugation steps were performed to separate the clay fractions. In specific cases, with low clay minerals volume, the decarbonation method was used. Quantitative identification of the main clay minerals was performed under air-dried, glycol-saturated, and heated treatments, using the Rietveld Method (Young, 1995). The mineralogy of the bulk samples was determined using a RIGAKU D/MAX-2200/PC diffractometer. The total mineralogical qualitative analysis was obtained using Jade 9 software (MDI) and the PDF-2 mineral database (ICDD).

PERIOD	STAGE	LOCAL STAGE	BASIN STAGE	STRATIGRAPHY		
				LAGOA FEIA GROUP		
LOWER CRETACEOUS	APTIAN	ALAGOAS	SAG	RETIRO Fm		
				ITABAPOANA Fm	GARGAU Fm	MACABU Fm
	BARREMIAN	JIQUIÁ	RIFT			
				ITABAPOANA Fm	COQUEIROS Fm	
		ARATU		ATAFONA Fm		

Fig. 2. Stratigraphic section of the study area with the Lagoa Feia Group (modified from Winter et al., 2007; Herlinger Jr. et al., 2017).

4. Results

4.1. Rift section lithofacies

Bioclastic grainstones and rudstones, stevensitic ooidal arenites, and dolostones are the main lithologic types in the rift interval (Fig. 3). Table 1 shows the average and maximum amounts of the main primary

(detrital, biogenic and syngenetic, chemically precipitated) and diagenetic constituents, as well as the pore types in each of these lithologic types, which were analyzed in the Coqueiros Formation. The average petrographic porosity is higher in the rift deposits. Bioclastic grainstones display the highest porosity values, followed by dolostones, stevensitic ooidal arenites and bioclastic rudstones (Table 1). Fracture and breccia porosity types are relatively more important in the stevensitic arenites

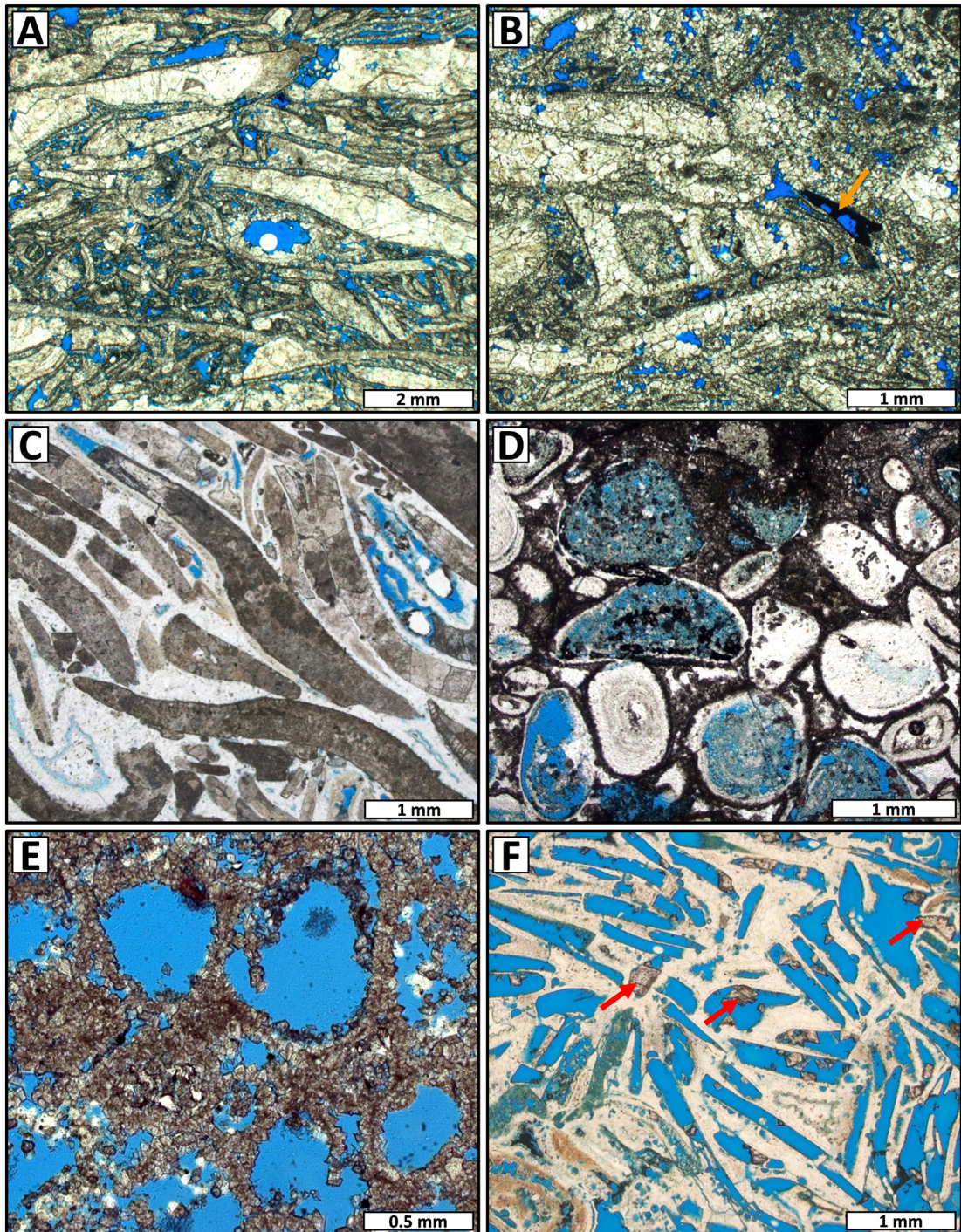


Fig. 3. Photomicrographs highlighting the main features of primary and diagenetic constituents and the porosity of rift-section deposits. A) Rudstone of fragmented, partially dissolved bivalve bioclasts, with well-preserved interparticle and intraparticle pores (blue) (uncrossed polarizers; //P); B) Bivalve-gastropod rudstone with interparticle porosity partially filled by bitumen (orange arrow) (//P). Note the bioclasts were partially neomorphosed, dissolved, and further cemented by calcite mosaic (//P); C) Rudstone of dolomitized bivalve bioclasts with interparticle pores intensely cemented by quartz (white) (//P); D) Stevensitic ooids and peloids completely dissolved and silicified (white) in stevensitic ooidal arenite (//P); E) Moldic and intercrystalline porosity in dolomitized stevensitic ooidal arenite (//P); F) Bioclastic rudstone with intraparticle and moldic pores partially cemented by saddle dolomite (red arrows). Silica cement (white) fills interparticle pores (//P).

Table 1

Statistical summary of the average and maximum (in brackets) amounts of major detrital and syngenetic primary constituents, diagenetic constituents, and pore types in the main defined lithologic types of the rift section in the study area.

RIFT STAGE		Bioclastic grainstones	Bioclastic rudstones	Stevensitic ooidal arenites	Dolostones
Lithologic types	Paragenetic relation				
Constituents (%)					
Detrital primary (total)		0.51 (0.67)	3.49 (21.67)	1.25 (2.33)	0.52 (2.00)
Mg-clay	Syngenetic	–	–	–	0.67 (3.33)
Calcite	Recrystallized bioclasts	10.57 (27.33)	14.52 (40.33)	–	–
	Replacing primary constituent	0.36 (1.33)	1.63 (18.00)	0.08 (0.33)	–
	Replacing diagenetic constituent	1.62 (3.67)	2.96 (69.67)	0.33 (1.33)	0.04 (0.33)
	Filling primary porosity	2.17 (5.00)	12.37 (29.33)	–	–
	Filling secondary dissolution porosity	5.73 (8.33)	20.02 (47.00)	0.17 (0.67)	0.11 (1.00)
Dolomite	Replacing primary constituent	39.59 (69.33)	11.36 (75.67)	21.29 (38.33)	15.52 (70.33)
	Replacing syngenetic constituent	–	–	–	–
	Replacing diagenetic constituent	–	0.21 (3.33)	5.04 (10.00)	36.35 (87.00)
	Filling primary porosity	10.34 (15.00)	2.97 (14.67)	6.84 (12.33)	–
	Filling secondary dissolution porosity	5.32 (7.00)	3.35 (15.33)	4.08 (14.33)	9.89 (28.33)
	Filling fracture porosity	–	0.22 (5.33)	–	–
Microcrystalline silica	Replacing primary constituent	1.52 (4.67)	0.85 (20.33)	19.59 (60.67)	–
	Replacing diagenetic constituent	–	2.11 (11.00)	7.48 (20.67)	1.74 (8.67)
	Filling primary porosity	–	1.01 (15.67)	5.09 (19.00)	–
Chalcedony	Filling secondary dissolution porosity	0.47 (1.67)	0.39 (1.67)	0.42 (1.67)	–
	Replacing primary constituent	0.34 (1.00)	0.42 (9.00)	–	–
	Replacing diagenetic constituent	–	0.51 (11.67)	0.33 (1.33)	0.44 (2.33)
	Filling primary porosity	–	0.56 (7.00)	2.42 (9.67)	–
Quartz	Filling secondary dissolution porosity	0.21 (0.67)	0.34 (2.33)	0.58 (2.33)	1.04 (7.33)
	Filling fracture/breccia porosity	–	0.76 (2.67)	–	–
	Replacing primary constituent	–	0.19 (0.67)	0.58 (2.33)	–
	Replacing diagenetic constituent	0.33 (0.67)	0.41 (2.67)	1.17 (3.00)	2.04 (7.33)
	Filling primary porosity	–	1.37 (26.33)	3.09 (6.00)	–
Pyrite/chalcopyrite/galena	Filling secondary dissolution porosity	1.47 (2.67)	1.89 (34.00)	1.81 (3.67)	8.03 (35.00)
	Replacing primary constituent	0.18 (0.33)	0.05 (0.67)	0.34 (0.67)	–
	Replacing syngenetic constituent	–	0.37 (1.67)	0.27 (0.67)	0.70 (2.67)
Sr-barite/celestine	Filling secondary dissolution porosity	–	0.21 (1.33)	–	0.33 (1.00)
	Replacing diagenetic constituent	–	0.86 (2.67)	–	1.07 (7.67)
	Filling secondary dissolution porosity	0.77 (1.33)	0.99 (3.33)	–	0.65 (2.33)
Svanbergite	Filling fracture porosity	–	–	–	2.66 (24.33)
	Replacing diagenetic constituent	0.18 (0.33)	–	0.35 (1.33)	0.22 (1.00)
Bitumen	Filling secondary dissolution porosity	–	0.36 (2.00)	–	–
Interparticle porosity	Filling secondary dissolution porosity	0.22 (0.33)	0.39 (1.67)	–	0.33 (1.33)
Primary porosity (total)	Primary	1.93 (3.67)	2.58 (6.00)	0.97 (1.67)	–
Intercrystalline porosity	Primary constituent dissolution	8.41 (10.33)	2.20 (6.67)	3.24 (4.67)	7.19 (11.67)
Intraparticle porosity	Diagenetic constituent dissolution	–	0.31 (3.33)	1.75 (3.33)	1.97 (5.33)
Moldic porosity	Diagenetic constituent dissolution	–	–	–	1.22 (4.33)
Vug porosity	Primary constituent dissolution	–	0.27 (3.00)	1.67 (3.67)	–
	Primary constituent dissolution	7.16 (10.00)	4.17 (7.67)	5.32 (9.00)	2.72 (8.00)
	Diagenetic constituent dissolution	–	0.13 (2.67)	–	1.02 (4.67)
Channel porosity	Primary constituent dissolution	0.83 (1.67)	1.94 (4.00)	3.15 (7.00)	2.85 (7.33)
Secondary dissolution porosity (total)	Diagenetic constituent dissolution	–	1.42 (3.67)	–	0.33 (2.67)
Fracture porosity	Diagenetic constituent dissolution	–	0.22 (1.33)	0.75 (2.67)	0.44 (3.33)
Breccia porosity	Primary constituent fracture	–	–	0.58 (1.33)	–
Fracture porosity (total)	Diagenetic constituent fracture	–	0.01 (0.33)	–	0.19 (1.67)
	Diagenetic constituent fracture	–	0.03 (0.67)	–	–
Total porosity (primary, secondary and fracture)		16.40	10.65	15.87	17.75
		18.33	13.27	17.42	17.94

than in the dolostones and bioclastic rudstones. The fracture apertures range from millimetric to centimetric and from totally unfilled to fully cemented.

4.1.1. Bioclastic grainstones and rudstones

The constituents of bioclastic grainstones and rudstones are mainly bivalves, ostracods, and gastropods (Fig. 3A, B, C). These deposits are commonly massive, locally slightly laminated, poorly to well sorted, and have a chaotic to subparallel orientation of the bioclasts. Partial to total recrystallization, dolomitization and/or silicification are common. Bivalves and ostracods present a wide variation in the degree of reworking and occur frequently fragmented but seldom strongly abraded. Bioclast grain size varies between 0.07 and 24.8 mm, with a mode of 2.3 mm. Intraclasts of clay ooids and peloids and microcrystalline

carbonate are very common, but in small amounts, and usually occur in the fine-grained sand size.

The main diagenetic processes in the bioclastic grainstones and rudstones are micritization of the margins of bioclasts, neomorphism, partial to complete recrystallization and dissolution of bioclasts. The inter- and intraparticle, intercrystalline, moldic, vugular, channel and fracture porosity were filled by drusy/rim pore-lining calcite, blocky and saddle dolomite, fibrous chalcedony, prismatic to coarse-crystalline mosaic quartz, and silica. They were also filled in smaller amount by prismatic celestine and Sr-barite, pyrite, svanbergite, and bitumen (Table 1; Fig. 3B, F). Svanbergite is a strontium and aluminum phosphate-sulfate that belongs to the APS group of the Woodhouseite series and has the chemical formula $\text{SrAl}_3(\text{PO}_4/\text{SO}_4)(\text{OH})_6$. The intensity of the neomorphism and dissolution of the bioclasts are highly variable,

Table 2

Statistical summary of the average and maximum (in brackets) amounts of major detrital and syngenetic primary constituents, diagenetic constituents, and pore types present in the main lithologic types of the sag section in the study area.

SAG stage		Fascicular calcite crusts	Claystones with calcite spherulites	Laminites	Intraclastic grainstones	Intraclastic rudstones	Dolostones	Cherts
Lithologic types	Paragenetic relation							
Constituents (%)								
Detrital primary (total)	–	0.91 (4.67)	–	8.79 (16.67)	16.72 (79.33)	17.81 (23.67)	0.05 (0.67)	–
Mg-clay	Syngenetic	0.53 (3.00)	0.53 (4.33)	2.96 (3.33)	0.20 (1.33)	0.75 (3.00)	0.86 (5.33)	0.07 (1.00)
Calcite	Fascicular crust covering/displaced syngenetic constituent	16.02 (53.67)	0.34 (1.67)	1.25 (5.00)	–	–	–	0.13 (1.33)
	Spherulite displacing syngenetic constituent	9.08 (22.33)	8.89 (12.33)	17.21 (39.33)	–	–	–	1.69 (11.33)
	Replacing primary constituent	–	–	–	15.27 (47.67)	5.25 (21.00)	–	–
	Replacing syngenetic constituent	0.56 (2.67)	–	4.12 (13.00)	1.13 (5.00)	–	–	–
	Replacing diagenetic constituent	3.40 (11.67)	2.34 (4.67)	–	2.26 (6.33)	–	1.14 (7.67)	1.13 (8.67)
	Filling primary porosity	3.33 (18.00)	–	–	0.93 (3.67)	–	–	0.32 (2.33)
	Filling secondary dissolution porosity	2.60 (13.33)	0.67 (2.33)	0.17 (0.67)	0.67 (3.33)	0.67 (1.67)	1.17 (4.33)	0.68 (4.00)
Dolomite	Filling fracture porosity	0.31 (3.33)	1.83 (4.00)	0.38 (1.33)	–	0.75 (3.00)	0.93 (3.00)	1.10 (3.67)
	Replacing primary constituent	–	–	5.50 (10.00)	25.05 (53.00)	13.59 (20.00)	24.42 (70.33)	4.37 (44.67)
	Replacing syngenetic constituent	4.84 (13.33)	2.17 (3.00)	19.50 (48.00)	1.03 (5.00)	0.50 (2.00)	5.76 (17.67)	1.55 (17.67)
	Replacing diagenetic constituent	6.16 (17.33)	9.47 (14.33)	18.25 (35.00)	2.67 (7.00)	3.04 (14.00)	19.64 (49.67)	7.09 (31.33)
	Filling primary porosity	2.78 (8.00)	0.34 (0.67)	–	8.74 (11.33)	1.75 (7.00)	–	–
	Filling secondary dissolution porosity	4.06 (25.67)	1.83 (3.67)	–	2.87 (12.67)	0.83 (1.67)	5.41 (14.00)	1.20 (5.33)
Magnesite	Filling fracture porosity	0.22 (2.67)	–	1.25 (5.00)	–	–	–	0.66 (3.67)
	Replacing syngenetic constituent	0.74 (2.33)	1.47 (2.67)	–	–	–	–	–
Microcrystalline silica	Replacing primary constituent	5.02 (23.67)	2.83 (3.33)	0.12 (0.67)	3.33 (16.67)	21.92 (46.67)	5.66 (32.00)	7.47 (34.33)
	Replacing syngenetic constituent	4.87 (15.67)	4.34 (8.00)	0.96 (3.00)	–	–	–	2.89 (17.67)
	Replacing diagenetic constituent	10.87 (31.67)	30.94 (36.33)	–	1.93 (9.67)	–	7.94 (31.67)	23.69 (49.33)
	Filling primary porosity	–	–	–	0.07 (0.33)	1.32 (5.33)	–	–
	Filling secondary dissolution porosity	0.33 (2.00)	–	–	–	0.51 (2.00)	0.76 (3.00)	0.56 (3.67)
Chalcedony	Filling fracture porosity	–	–	–	–	–	–	0.04 (0.67)
	Replacing primary constituent	–	–	–	–	2.92 (10.00)	–	–
	Replacing syngenetic constituent	0.22 (3.00)	0.17 (0.33)	2.50 (10.00)	–	–	–	0.31 (1.33)
	Replacing diagenetic constituent	3.16 (19.67)	4.51 (6.67)	–	–	–	2.02 (12.67)	10.93 (26.33)
	Filling primary porosity	0.04 (0.67)	0.34 (0.67)	–	0.53 (2.67)	1.59 (5.67)	–	0.18 (1.33)
	Filling secondary dissolution porosity	3.13 (11.33)	5.61 (9.00)	–	–	3.67 (10.33)	2.79 (14.00)	7.34 (26.33)
Quartz	Filling fracture porosity	–	–	–	–	–	–	0.04 (0.67)
	Replacing primary constituent	–	–	–	–	1.08 (3.00)	–	–
	Replacing syngenetic constituent	0.07 (0.67)	–	1.25 (5.00)	–	–	–	–
	Replacing diagenetic constituent	0.67 (4.67)	2.05 (3.33)	–	0.13 (0.67)	–	1.10 (3.67)	1.91 (7.33)
	Filling primary porosity	0.04 (0.67)	–	–	0.13 (0.67)	1.17 (3.67)	–	–
	Filling secondary dissolution porosity	3.71 (19.33)	9.04 (11.67)	0.25 (1.33)	2.27 (10.67)	9.03 (16.00)	3.36 (14.00)	13.79 (34.00)
Pyrite/chalcopyrite/galena	Filling fracture porosity	0.24 (3.67)	1.89 (4.00)	–	–	–	–	0.44 (5.67)
	Replacing primary constituent	0.07 (1.00)	–	0.52 (1.67)	0.25 (1.00)	0.59 (1.33)	–	–
	Replacing syngenetic constituent	0.38 (1.67)	0.34 (0.67)	12.36 (37.00)	0.12 (0.67)	–	0.10 (0.67)	0.02 (0.33)
	Replacing diagenetic constituent	0.47 (3.00)	–	1.77 (3.67)	0.17 (1.33)	0.33 (1.33)	0.57 (2.33)	0.13 (1.67)
	Filling primary porosity	0.93 (7.67)	0.17 (0.33)	–	–	–	–	0.04 (0.67)
	Filling secondary dissolution porosity	0.38 (4.33)	–	–	–	–	0.83 (2.67)	0.57 (2.00)
	Filling fracture porosity	0.04 (0.67)	–	–	–	–	–	0.11 (1.67)
Sr-barite/celestine	Replacing syngenetic constituent	–	–	0.91 (3.00)	–	–	–	–
	Replacing diagenetic constituent	–	–	–	–	–	0.39 (1.33)	0.45 (2.00)
	Filling primary porosity	0.54 (2.67)	–	–	–	–	–	–
	Filling secondary dissolution porosity	0.77 (3.33)	0.29 (1.00)	–	0.32 (1.33)	0.46 (1.67)	1.33 (4.00)	1.24 (3.67)
	Filling fracture porosity	–	–	–	–	0.11 (1.00)	0.59 (2.33)	0.98 (3.33)

Table 2 (continued)

SAG stage		Fascicular calcite crusts	Claystones with calcite spherulites	Laminites	Intraclastic grainstones	Intraclastic rudstones	Dolostones	Cherts
Lithologic types	Paragenetic relation							
Constituents (%)								
Sphalerite	Replacing primary constituent	–	–	–	–	0.68 (2.00)	–	–
	Replacing diagenetic constituent	0.27 (1.33)	0.42 (2.33)	–	–	–	–	–
	Filling secondary dissolution porosity	–	–	–	–	–	0.38 (2.33)	0.52 (2.67)
	Replacing primary constituent	–	–	–	–	0.42 (1.00)	–	–
Svanbergite	Replacing syngenetic constituent	0.59 (1.67)	–	–	–	–	0.19 (1.33)	–
	Replacing diagenetic constituent	0.94 (2.33)	0.72 (1.67)	–	–	–	–	0.86 (2.67)
	Filling secondary dissolution porosity	–	–	–	0.43 (1.67)	–	–	0.31 (1.33)
	Filling secondary dissolution porosity	–	–	–	0.73 (2.67)	–	–	–
Zeolite	Filling fracture porosity	–	–	–	–	–	–	–
Rutile	Filling secondary dissolution porosity	0.27 (2.00)	–	–	–	–	–	0.29 (2.33)
Bitumen	Filling secondary dissolution porosity	0.44 (1.67)	0.17 (0.67)	–	0.13 (0.67)	0.25 (1.00)	0.38 (1.33)	0.51 (1.67)
Interparticle porosity	Primary	–	–	–	1.87 (6.00)	0.55 (1.33)	–	–
Growth-framework porosity	Between syngenetic constituents	0.42 (1.67)	–	–	–	–	–	–
Primary porosity (total)		0.42	–	–	1.87	0.55	–	–
Mg-clay dissolution porosity	Syngenetic constituent dissolution	0.80 (2.33)	0.52 (1.67)	–	0.34 (1.67)	–	–	–
Intercrystalline porosity	Primary constituent dissolution	0.11 (1.33)	–	–	4.77 (9.67)	0.71 (3.00)	5.19 (15.00)	0.27 (3.00)
	Diagenetic constituent dissolution	1.30 (3.67)	1.14 (2.67)	–	–	1.03 (2.33)	1.19 (3.67)	0.60 (3.33)
Intra-crystalline aggregate porosity	Primary constituent dissolution	0.63 (2.33)	–	–	–	0.22 (0.67)	–	–
	Diagenetic constituent dissolution		0.17 (0.67)	–	–	–	0.33 (1.33)	0.51 (1.67)
Intraparticle porosity	Primary constituent dissolution	–	0.48 (1.33)	–	1.60 (4.67)	3.31 (6.00)	–	–
Moldic porosity	Primary constituent dissolution	–	–	–	1.47 (4.00)	0.72 (3.00)	1.86 (6.33)	–
Vug porosity	Primary constituent dissolution	2.27 (7.00)	1.20 (2.33)	–	1.87 (4.33)	2.32 (5.67)	3.24 (7.00)	1.64 (7.00)
Secondary dissolution porosity (total)		5.11	3.50	–	10.04	8.31	11.81	3.02
Fracture porosity (total)	Primary constituent fracture	0.44	2.83	–	–	0.17	0.43	1.24
Total porosity (primary, secondary and fracture)		5.98	6.33	–	11.90	9.03	12.24	4.26

as the amounts of intra-particle and moldic porosity generated by their dissolution. The bioclasts are heterogeneously replaced by dolomite, microcrystalline silica, quartz, chalcedony, and sulfides.

In some bioclastic grainstones and rudstones, coarse-crystalline saddle dolomite, calcite, Sr-barite, and celestine fill preferentially inter- and intraparticle, moldic, vugular, and fracture porosity (Fig. 3F). Silica phases are very common in the rift section (45.8% of the described samples), where they mainly replace the bioclasts, which may be partially to intensely silicified. Quartz occurs preferentially as prismatic rims and as a coarse mosaic of crystals within inter- and intraparticle porosity (Fig. 3C, F).

4.1.2. Stevensitic ooidal arenites

Another lithologic type characteristic of the rift section is arenites constituted by ooids of syngenetic magnesian layer silicates (mostly stevensite; see Supplementary material) (Fig. 3D). The rift stevensitic ooidal arenites present a massive to slightly laminated structure with good to moderate sorting and stevensite ooids in sizes ranging between 0.3 and 1.7 mm, with a mode of 0.7 mm. As described by Herlinger Jr. et al. (2017), the stevensitic ooidal arenites occurring at the top of the rift section of the northern Campos Basin are usually deformed, fractured, dissolved, and replaced by silica, calcite, dolomite and quartz.

The stevensitic ooids were partially to totally replaced by blocky or mosaic calcite and dolomite, prismatic and mosaic quartz, fibrous chalcedony, microcrystalline silica (Fig. 3D), pyrite, and svanbergite. The interparticle, intraparticle, intercrystalline, moldic (Fig. 3E), vugular,

channel, and fracture porosity are generally filled by calcite as fibrous and microcrystalline rims, botryoidal, fine- to coarse-crystalline, and mosaic to drusy, as well as by silica, chalcedony, quartz and dolomite (Table 1). Silica and blocky and/or mosaic dolomite selectively replaced the peloids partially to totally.

4.1.3. Dolostones

Dolostones correspond to 15.9% of the samples described in the rift interval. However, some dolomitization was observed in 59.7% of the analyzed rift samples, varying from incipient to very intense. Some degree of fracturing was identified in 14.3% of the dolostone samples. The crystal sizes in the rift dolostones range between 0.01 (very fine crystallinity) and 1.57 mm (medium crystallinity), with a modal size of 0.16 mm. The protolith was recognizable in 24.1% of the rift dolostones. Of these, 57.1% correspond to bioclastic rudstones, 14.3% to grainstones and 28.6% to stevensitic ooidal arenites (Fig. 3E).

Pore types in the rift dolostones are exclusively secondary, of intercrystalline, intracrystalline, moldic, vugular, channel, and fracture types. The main diagenetic phases that replace primary and diagenetic constituents and fill the porosity are mosaic calcite, blocky and saddle dolomite (Fig. 3F), quartz prismatic rims to drusiform, fibro-radiated and rims chalcedony, and silica. Secondary constituents were svanbergite, Sr-barite, celestine, euhedral to subhedral sulfides (pyrite, chalcopyrite and galena), and bitumen (Table 1). Another important diagenetic feature that was observed in some of the analyzed samples from the Macabu and Coqueiros Formations is the presence of stylolites, some of them had

dissolution halos (10.2% of the samples) and occur frequently associated with dolomitized intervals and residual concentrations of pyrite.

4.2. Sag phase lithofacies

The main lithologic types recognized in the sag section (Macabu Formation) are fascicular calcite crusts, stevensitic claystones with calcite spherulites (see Supplementary material), intraclastic rudstones and grainstones, laminites, dolostones, and cherts. Table 2 shows the average and maximum amounts of the main primary (detrital, syngenetic, and chemically precipitated) and diagenetic constituents, as well as the pore types in each of these lithologic types that were analyzed in the Macabu Formation.

Primary porosity in the fascicular calcite crusts is essentially of the growth-framework (inter-crystalline aggregate) type (Table 2). Secondary porosity is notably dominant in the analyzed sag rocks, accounting for 95.9% of total petrographic porosity on average. The matrix dissolution, laminar, intraparticle, intercrystalline, moldic, vugular, intra-crystalline aggregate, and fracture secondary porosity were identified. The lithologic types with a higher average petrographic porosity are dolostones and intraclastic grainstones and rudstones, followed by spherulitic rocks, fascicular calcite crusts, and cherts. The fracture porosity is relatively more important in spherulitic rocks and cherts, and secondarily in fascicular calcite crusts, dolostones, and intraclastic rudstones (Table 2).

4.2.1. Fascicular calcite crusts

Laminations in the studied fascicular calcite crusts range in thickness from 0.4 to 5.2 mm, with a mode of 1.8 mm (Fig. 4A, B). Such crusts are intercalated with discontinuous levels formed by laminations, peloids and clay ooids and siliciclastic grains, such as muscovite and quartz, which were partially to totally replaced by dolomite, calcite, microquartz, chalcedony, and pyrite. The clay peloids that were partially replaced by calcite or silica also commonly appear included in the fascicular aggregates. Approximately 16% of the analyzed crusts show good preservation of the original fascicular habitat (Fig. 4C). The remainder present different types of recrystallization (in sectors, in mosaic, with and without preservation of optical orientation); dolomitization (microcrystalline, blocky and saddle dolomite); and silicification (microcrystalline silica, chalcedony spherulites, and blocky, mosaic, and prismatic quartz) (Table 2).

In the fascicular calcite crusts, the pore types that occur are primary (growth-framework, inter-crystalline aggregates) and secondary (Mg-clay dissolution, intercrystalline and intra-crystalline aggregates, vugular, and fracture). The most common diagenetic phases that replace preexisting constituents and fill the porosity in calcite crusts are blocky, baroque and saddle dolomite; fine-to-thick mosaic and prismatic rims calcite; flamboyant, prismatic rims to drusiform quartz; and silica (Fig. 5A). Fibrous, fibro-radiated and spherulitic chalcedony; microcrystalline, pseudocubic svanbergite (Fig. 5A); sulfates; sulfides; and magnesite occur in a subordinate amount (Table 2). Furthermore, dolomite, lamellar, pseudomorphic magnesite and microcrystalline silica also commonly occur in replacing the stevensite laminations.

However, macrocrystalline quartz and calcite (Figs. 5C, D, 6); radiated and oriented Sr-barite and celestine (Fig. 5B, C, D); prismatic sphalerite (Fig. 5E, F); pyrite, chalcopyrite and galena (Fig. 6E, F); fibro-radiated zeolite (Fig. 6C, D); chlorite; rutile; and massive bitumen with shrinkage cracks were only found filling the growth framework, Mg-clay dissolution, intercrystalline, intra-crystalline aggregate, vugular, and fracture porosity (Table 2; Fig. 7). Prior to the precipitation of saddle dolomite, quartz, calcite, sulfates, sulfides, zeolite, rutile, and bitumen, important fracturing and dissolution events occurred, which largely modified the pre-existing pore systems (Fig. 7B, C, E, F). In many samples, the saddle dolomite dissolution occurs preferably on the inside of the crystals, thereby creating important intracrystalline porosity (Fig. 7A).

Euhedral to subhedral, 0.05 to 5 mm crystals of Sr-barite, celestine, pyrite, sphalerite, chalcopyrite and galena occur filling vugular pores and fractures, often with a poikilotopic texture replacing and engulfing dolomite, calcite and quartz (Fig. 7F). Paragenetic relationships with macrocrystalline calcite, quartz and sphalerite, and radiated chalcedony partially engulf and replace saddle dolomite and Sr-barite. The SrO content in the analyzed Sr-barite ranges from 2% to 16%, with an average of 6.7% (WDS analysis). Aggregates of microcrystalline rutile were identified filling vugular and fracture porosity, which were associated with native copper (Cu) and zinc (Zn) (Fig. 7E). Solid bitumen commonly occurs partially filling the secondary porosity, which generally represents the last phase of this paragenesis (Fig. 7B). In addition, fluorite and dickite have also been described in other wells of the study area (Herlinger Jr. et al., 2017), and dawsonite was identified in the XRD analysis (see Supplementary material).

4.2.2. Stevensitic claystones with calcite spherulites

The syngenetic laminated deposits constituted by magnesian layer silicate phases, probably of stevensitic original composition, with some kerolite (Supplementary material; Figs. 4D, E, F, 8A, B), form a significant part of the Aptian Macabu Formation. Commonly, only a small proportion of the Mg-clays is preserved in the thin sections, making their recognition very difficult. Mg-clay deposits were widely dissolved and/or replaced by dolomite, microcrystalline silica, chalcedony, quartz, pyrite and svanbergite (Table 2). The pseudomorphic replacement of stevensite by magnesite is also very common. In addition, a pyritization process of the portion that was originally composed of the stevensite clay matrix was also verified. Calcite spherulites, which were characterized as approximately symmetrical fibro-radiated aggregates (Hodgson, 1968; Schroeder, 1972; Chafetz and Butler, 1980; Verrecchia et al., 1995), occur conspicuously replacing and displacing the irregularly laminated Mg-clay deposits (Fig. 4E, F). The diameter of calcite spherulites range between 0.2 and 2.7 mm, with a mode of 0.9 mm (Fig. 8A, B). Some spherulites present nuclei formed by ostracod bioclasts or clay peloids.

Transitional forms between spherulitic and fascicular aggregates were found in many samples, including asymmetrical spherulites, vertically elongated spherulites with lobate borders, hemispherulites, and single or multiple fascicular aggregates nucleated on spherulites. Another relevant aspect of the analyzed samples is the very good preservation of the fibrous habit of original calcite crystals in many of the fascicular calcite crusts and calcite spherulites (Fig. 8A, B), which are currently composed of non-magnesian calcite. Partially to totally dolomitized and silicified calcite spherulites with the Mg-clay matrix mimetically replaced by dolomite commonly occur (Figs. 4E, F, 8A, B).

Pore types in the spherulitic rocks are only secondary and occur from matrix dissolution, inter- and intra-crystalline aggregates, intraparticle, vugular (Fig. 7C), and fracture. Stevensitic claystones replaced by calcite spherulites and dolomite commonly present low porosity, but locally abundant secondary pores were generated by stevensite dissolution. The typical diagenetic phases that replace primary and diagenetic constituents as cement filling porosity in spherulitic rocks are blocky, baroque and saddle dolomite; calcite as bladed crystals and fine-to-coarse mosaic; quartz as prismatic rims; fibrous and spherulitic chalcedony; and silica. Secondarily by svanbergite, sulfates, sulfides, magnesite, and bitumen (Table 2).

4.2.3. Laminites

The Aptian laminites (sag section) analyzed in this study present a range of lamination types with thicknesses varying usually from millimeter to centimeter, and with shapes varying from simple planar to wavy (Fig. 8C, D), as described by Coniglio et al. (2004) for laminites of the Upper Silurian in the Michigan Basin. Most laminated deposits are characterized by thin horizontal to sub-horizontal, mostly isopachous laminations that range from regular to discontinuous and that are commonly crenulated. The apparently crenulated contacts observed in some

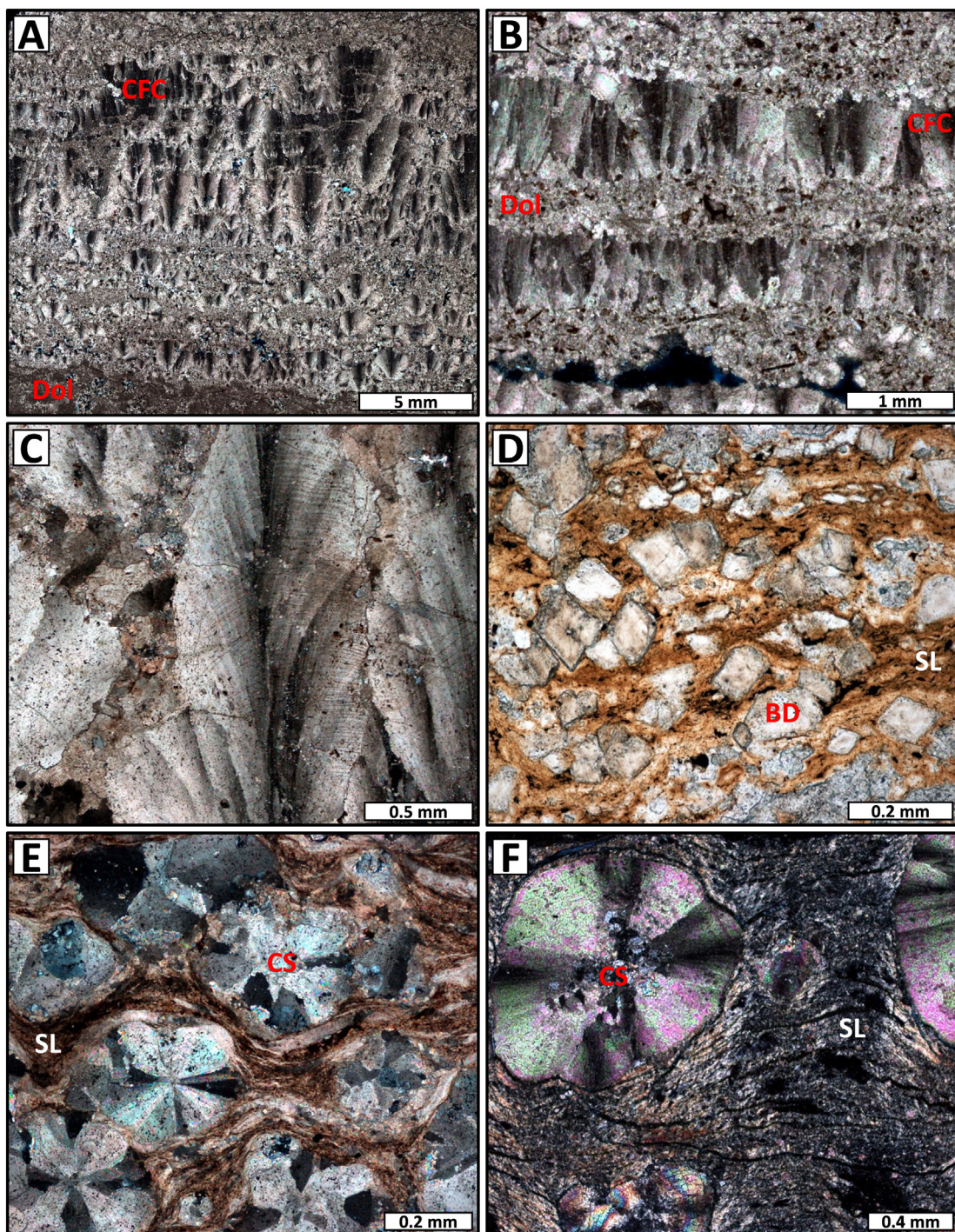


Fig. 4. Photomicrographs highlighting main features in syngenetic and diagenetic constituents of the sag section. A) and B) Fascicular-optic calcite crusts (CFC) intercalated with granular deposits replaced by dolomite (Dol) (crossed polarizers; XP); C) Divergent calcite crystal aggregates with fascicular-optic texture (XP); D) Stevensite laminations (SL) replaced and displaced by blocky dolomite (BD) (uncrossed polarizers; //P); E) Calcite spherulites in the laminated Mg-clay matrix (SL) replaced by dolomite (XP); F) Partially silicified calcite spherulites (CS), displacing and replacing Mg-clay laminations (SL) (XP).

laminites could indicate a possible microbial origin but under petrographic observation are revealed to correspond to microstylolites.

The most abundant constituents of the laminites are calcite and dolomite (Table 2). Detailed observations reveal that most laminites correspond originally to laminated clays deposits, probably stevensitic, which were extensively replaced by calcite or dolomite (Fig. 8D). Remnants of the original clays are marked by organic matter and siliciclastic grains (quartz, biotite and muscovite). Other levels are

intensely silicified, exhibit secondary dissolution porosity, and are partially filled by carbonate and siliceous cements. Replacement by calcite, dolomitization and silicification range from complete to selective alteration of individual laminae. Sparse calcite spherulites and nodular structures that are asymmetrical and often coalesced occur commonly.

The most common diagenetic phases replacing primary and diagenetic constituents in the laminites are microcrystalline, blocky and fine mosaic calcite and dolomite; microcrystalline silica; fibrous

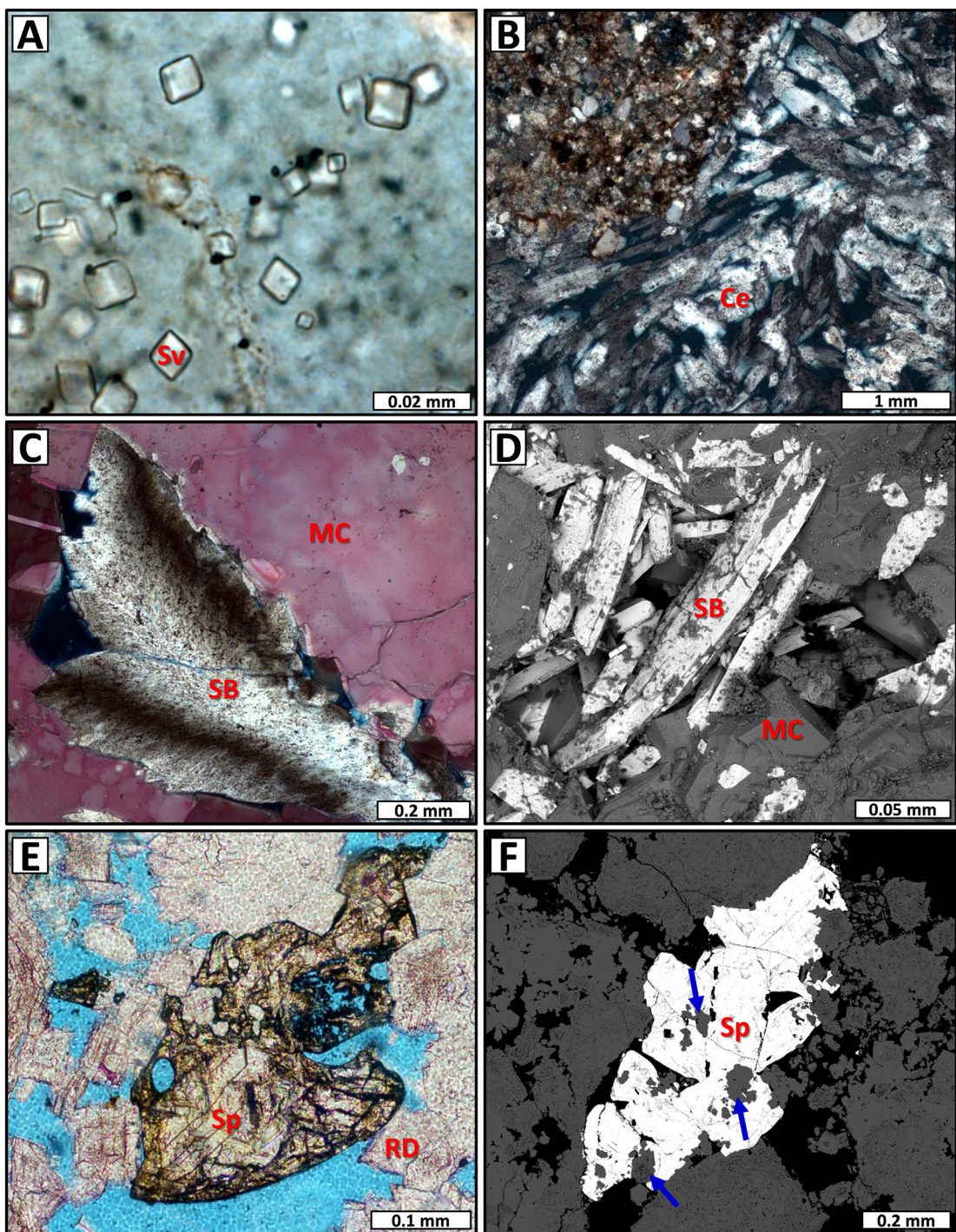


Fig. 5. Petrographic features of svanbergite, Sr-barite, and sphalerite. A) Microcrystalline pseudocubic svanbergite (Sv) crystals immersed in chert constituted by microcrystalline silica (//P); B) Prismatic, elongated and oriented celestine (Ce) crystals filling fracture porosity and partially replacing dolomite in dolostone (XP); C) Radiated Sr-barite (SB) and macrocrystalline calcite (MC) (stained red) filling vugular pore (XP); D) Elongated prismatic Sr-barite (SB) and euhedral macrocrystalline calcite (MC) partially filling the vugular porosity (BSE); E) Macrocrystalline, partially dissolved sphalerite (Sp) and rhombohedral dolomite (RD) partially filling the vugular pore (//P); F) Macrocrystalline sphalerite (Sp) engulfing and replacing dolomite (blue arrows) and partially filling vugular porosity (BSE).

chalcedony; and quartz. Blocky, frambooidal and microcrystalline pyrite; and radiated Sr-barite also occur in smaller amounts (Table 2). The porosity of the laminites is very low, and the pores are secondary, from matrix dissolution, with minor laminar pores, intercrystalline among blocky dolomite or quartz, and microfractures that are partially filled by blocky to mosaic calcite, dolomite and quartz. Styolites and relatively well preserved ostracods are also common.

4.2.4. Intraclastic grainstones and rudstones

The constituents of intraclastic grainstones and rudstones (Fig. 8E, F, respectively) are mainly fragments of reworked calcite crusts, calcite spherulites, Mg-clay laminated aggregates, and laminated carbonates. Massive to stratified intraclastic grainstones and rudstones that are locally slightly compacted and cemented may show good porosity and permeability. The intraclast grain size varies between 0.06 and

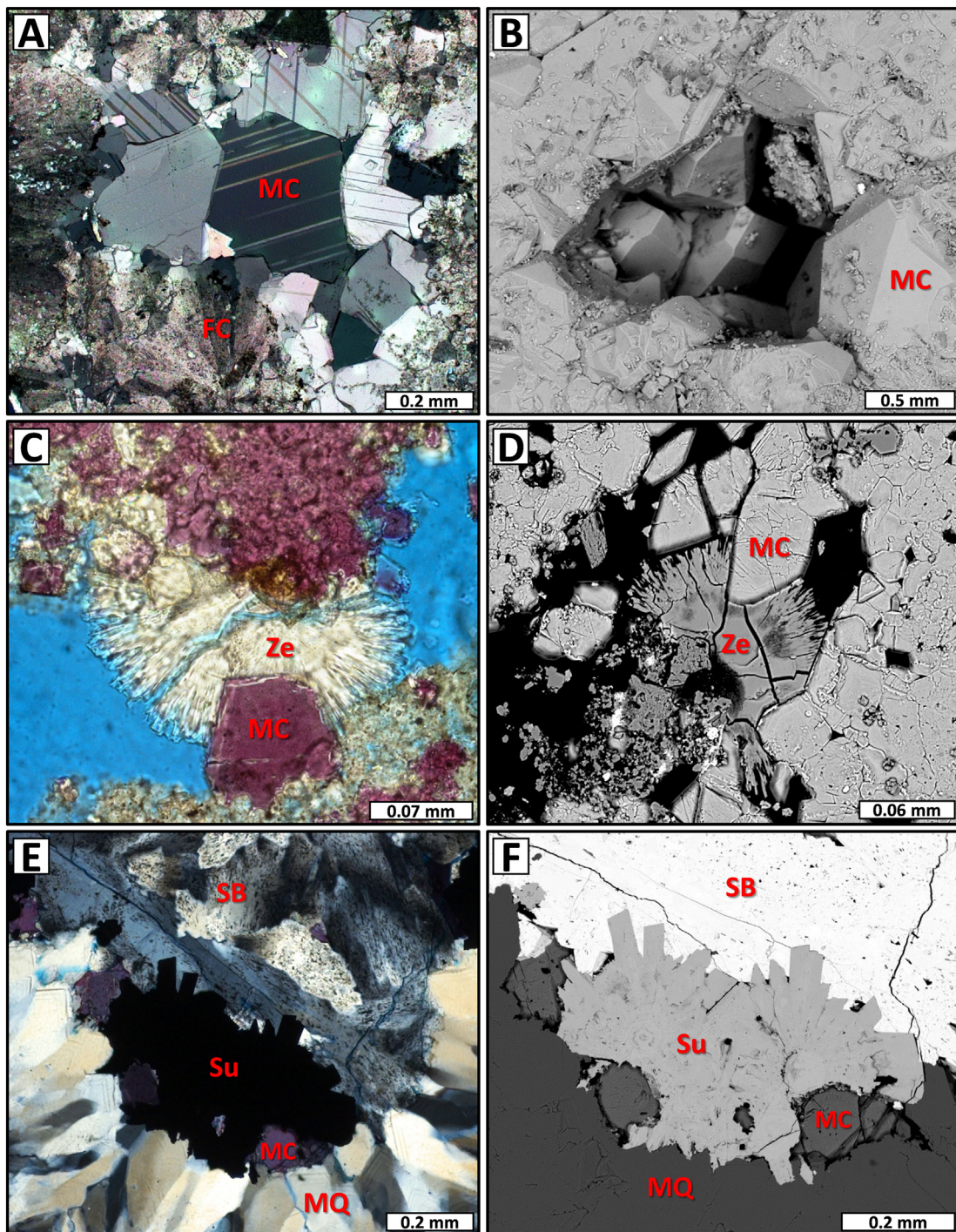


Fig. 6. Aspects of macrocrystalline calcite, zeolite and sulfides. A) Twinned macrocrystalline calcite (MC) completely filling vugular porosity in fascicular calcite crust (FC) (XP); B) Drusiform macrocrystalline calcite (MC) partially cementing the vugular pore in chert. Secondary electrons microscopy (SEM) image; C) Fibro-radiated zeolite (Ze) and euhedral macrocrystalline calcite (MC) (stained red) filling the vugular porosity in intensely recrystallized and dolomitized intraclastic grainstone (//P); D) Fibro-radiated zeolite (Ze) and euhedral macrocrystalline calcite (MC) filling partially vugular pores in chert (BSE); E) and F) Euhedral sulfides (Su) (mostly pyrite, secondarily chalcopyrite and galena), lamellar Sr-barite (SB), macrocrystalline calcite (MC) and prismatic macroquartz (MQ) filling vugular and fracture porosity in chert (XP and BSE, respectively).

4.1 mm, with a modal size of 0.8 mm. According to Herlinger Jr. et al. (2017), some intraclastic rocks contain a redeposited clay matrix and, therefore, should be considered hybrid rocks.

The main pore types in intraclastic grainstones and rudstones are primary interparticle and secondary from the dissolution of Mg-clay matrix, intercrystalline, intraparticle, moldic, vugular, and fracture. The diagenetic phases that commonly replace preexisting constituents and fill the porosity in intraclastic rocks are calcite as mosaic

aggregates and prismatic rims, blocky and saddle dolomite, prismatic rims to drusiform quartz, spherulitic chalcedony, and silica. Svanbergite, sulfates, sulfides, fibro-radiated zeolite (Fig. 6C), and bitumen are less common (Table 2). The analyzed zeolite has 8.9% K₂O, 0.7% CaO, 0.4% F, 0.3% SrO, and 0.1% BaO (WDS analysis). Compaction was intense along the interparticle contacts, both through mechanical (grain fracturing and deformation) and chemical (pressure dissolution) processes.

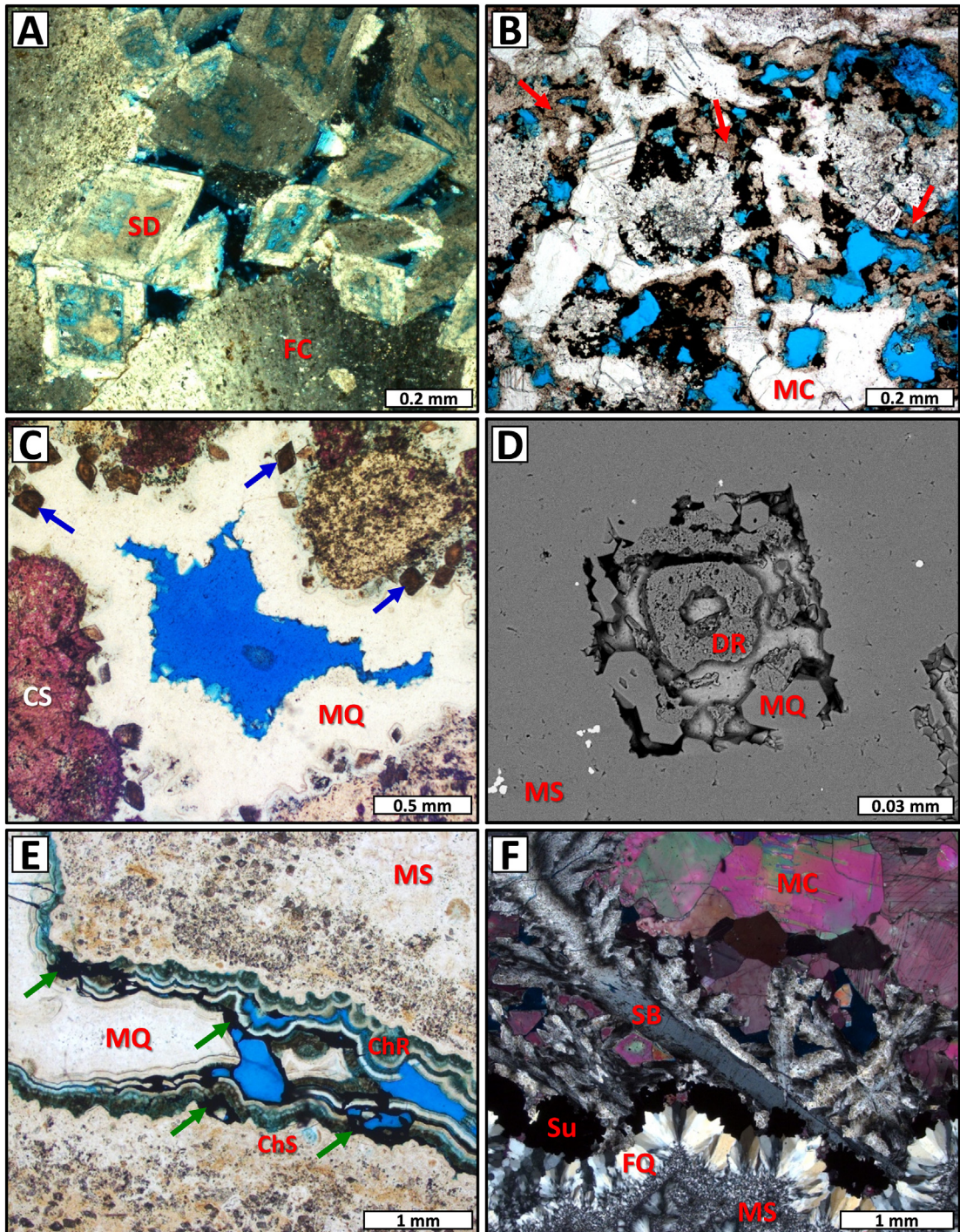


Fig. 7. Examples of pores and cements in the studied samples. A) Intracrystalline porosity in zoned saddle dolomite (SD) filling growth-framework porosity in fascicular calcite crust (FC) (XP); B) Bitumen (black), macrocrystalline calcite (MC) and dolomite (red arrows) partially filling the vugular porosity (blue) in chert (//P); C) Vugular porosity partially cemented by macrocrystalline quartz (MQ), partially silicified rhombohedral dolomite (blue arrows) and calcite spherulites (CS) (stained red) (//P); D) Detail of intracrystalline porosity in partially preserved dolomite rhomb (DR) intensely replaced by microcrystalline silica (MS) and macrocrystalline quartz (MQ) (BSE); E) Fracture porosity partially filled by euhedral macrocrystalline quartz (MQ), chalcedony rims (ChR) and microcrystalline rutile (green arrows) in chert constituted by microcrystalline silica (MS) and chalcedony spherulites (ChS) (//P); F) Vugular porosity completely cemented by microcrystalline silica (MS), flamboyant quartz (FQ), opaque sulfides (Su) (pyrite, chalcopyrite and galena), radiated Sr-barite (SB), and macrocrystalline calcite (MC) (XP).

4.2.5. Dolostones

Dolostones represent 11.5% of the samples described in the sag section (Fig. 9). However, some dolomitization was observed in 69.1% of the analyzed sag samples, varying from incipient to very intense. In 14.3% of the dolostone samples, some intensity of fracturing was identified. The main diagenetic phases replacing preexisting

constituents and filling porosity in the sag dolostones are microcrystalline, blocky (Fig. 9A, B, D), fine mosaic and saddle (Fig. 9C, E, F) dolomite; mosaic calcite; fibrous and laminated to botryoidal chalcedony; drusiform quartz; and silica (Fig. 9B, F). Secondly, they are replaced by Sr-barite, celestine, sulfides, svanbergite, and bitumen (Table 2). These phases fill intra-crystalline aggregate, clay matrix

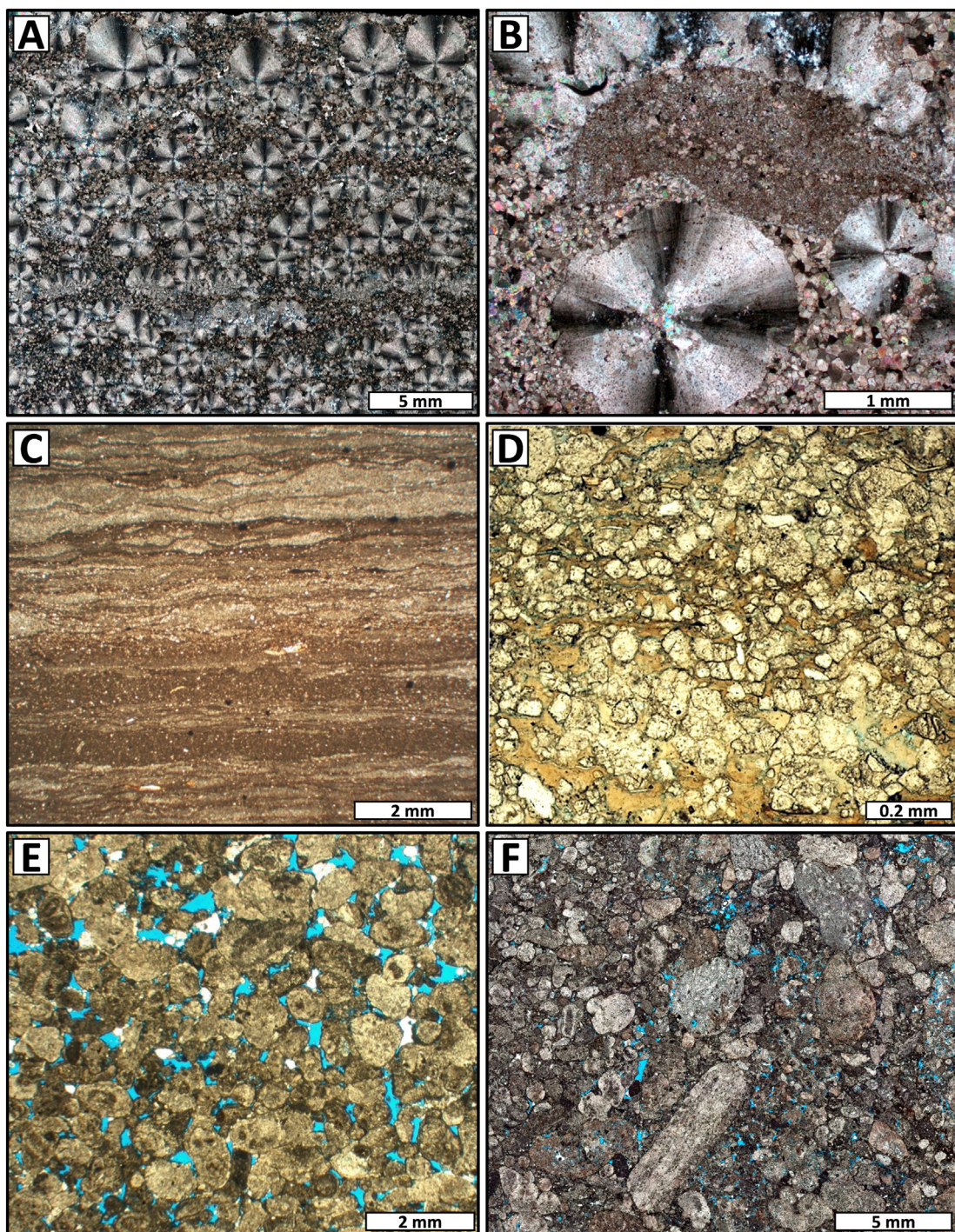


Fig. 8. Main features in diagenetic, detrital, and pore constituents in sag lithologic types. A) Calcite spherulites in the Mg-clay matrix replaced by microcrystalline dolomite (XP); B) Partially dolomitized calcite spherulites (CS) with stevensite replaced by dolomite (XP); C) Planar to wavy laminite with millimetric laminations defined by the predominance of clay and of microcrystalline dolomite (//P); D) Dolomite extensively replacing the original Mg-clay matrix in laminite (//P); E) Intraclastic grainstone with well-preserved interparticle porosity (blue) (//P); F) Intraclastic rudstone with interparticle porosity partially cemented by calcite and dolomite (//P).

dissolution, laminar, intercrystalline, moldic, vugular, and fracture secondary porosity (Fig. 9). The crystal sizes in the sag dolostones range between 0.01 (very fine crystallinity) and 3.27 mm (medium crystallinity), with a modal size of 0.09 mm.

Dolomite with microcrystalline and blocky habits partially and heterogeneously replaced the Mg-clay matrix, as well as the calcite spherulites and fascicular aggregates (Fig. 10). In many samples, dolomite selectively replaced the stevensitic sediments, while the

calcite aggregates are only marginally dolomitized (Fig. 10C). The original deposits that were modified by dolomitization and silicification processes were difficult, if not impossible, to recognize. In some partially dolomitized rocks, dolomitization occurred only at the edges of fascicular and spherulitic calcite, appearing as microcrystalline dolomite that partially followed the divergent optical calcite orientation (Fig. 11A).

Dolomite with orange cathodoluminescence (CL) patterns replaced the Mg-clay sediments, as well as the fascicular and spherulitic calcite

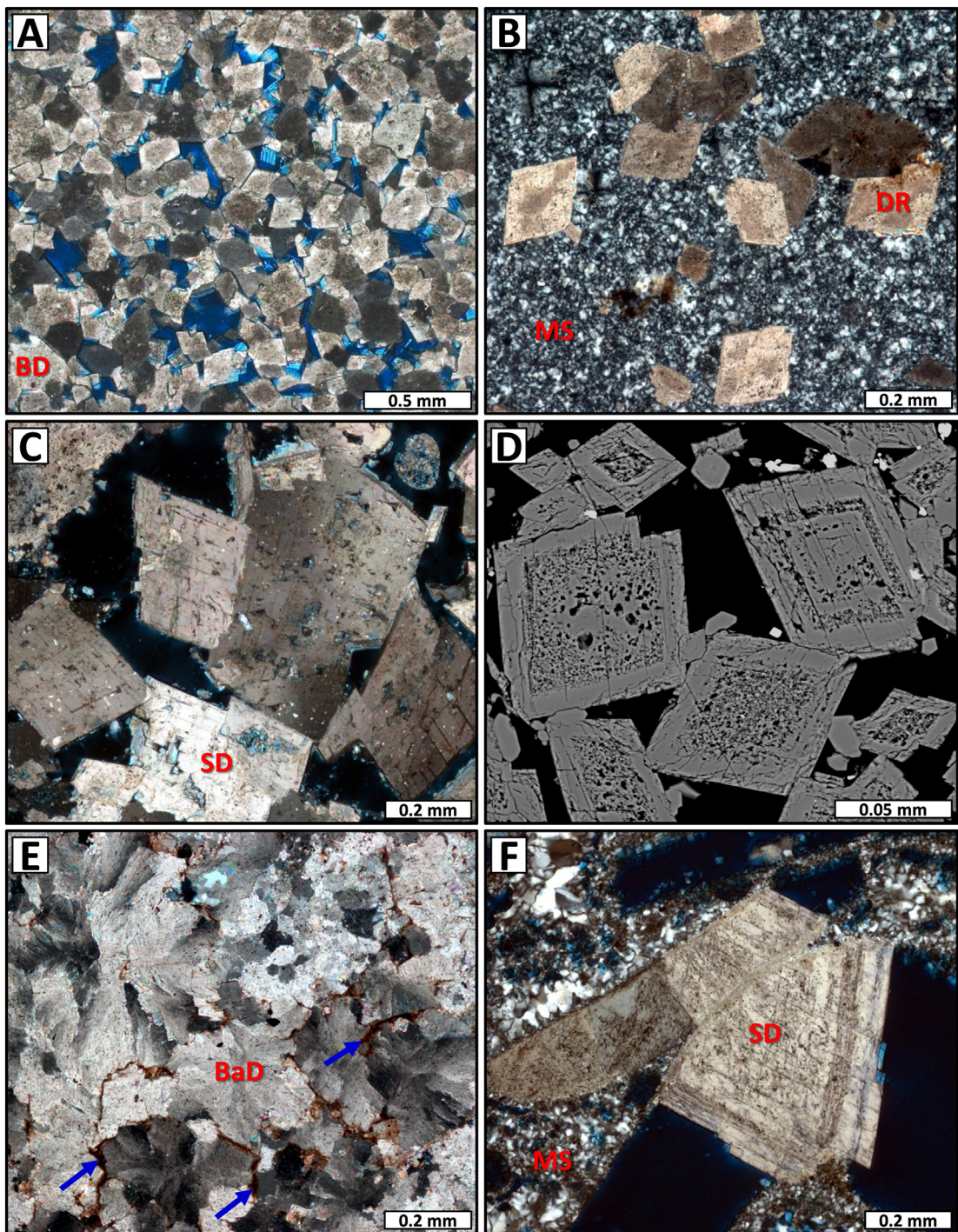


Fig. 9. Aspects of dolomite in sag dolostones and other strata affected by dolomitization. A) Dolostone with blocky dolomite (BD) and intercrystalline porosity (XP); B) Dolomite rhombs (DR) in rock intensely replaced by microcrystalline silica (MS) (XP); C) Partially dissolved saddle dolomite (SD) crystals filling the vugular pore (XP); D) Dolomite rhombohedra with well-developed zonation defined by fluid inclusions, cementing fracture porosity (backscattered electrons image, BSE). Note the selective dissolution in the center of the dolomite rhombs; E) Dolostone composed of baroque dolomite (BaD) replacing non-selectively clays and other constituents, and filling vugular porosity (XP). Remnants of brown magnesian clay (blue arrows) among baroque dolomite aggregates; F) Zoned saddle dolomite (SD) filling vugular porosity in silicified intraclastic rudstone (XP).

aggregates (red CL) (Fig. 11A). In addition, dolomite rhombohedra occur partially filling inter-aggregate pores in the fascicular crusts and those formed by the dissolution of the syngenetic Mg-clay matrix. Such dissolution generated the laminar and vugular porosity that were observed in part of the sag samples. Magnesite occurs in some samples, pseudomorphically replacing part of the stevensitic matrix laminations (EDS, WDS and XRD analyses; Supplementary material).

4.2.6. Cherts

Totally silicified rocks (cherts) were only observed in the sag section, corresponding to 27.4% of the described sag samples (Fig. 12). These rocks are constituted by microcrystalline and macrocrystalline silica, quartz as prismatic rims and mosaics, and chalcedony as fibrous rims and spherulitic aggregates, which partially to fully replaced the pre-existing constituents and filled secondary pores (Table 2). In the

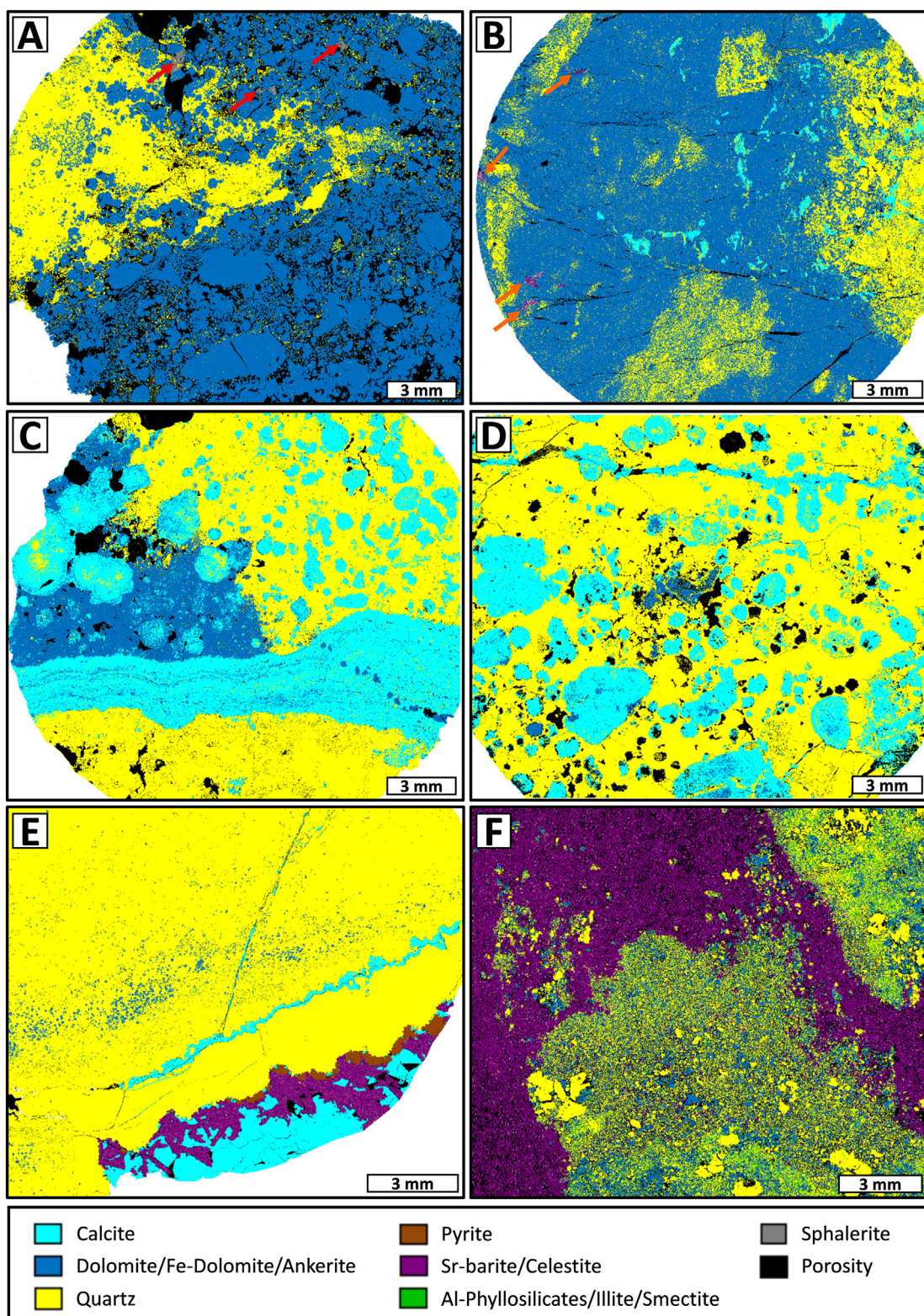


Fig. 10. QEMSCAN images showing structural, textural, and fabric features that are characteristic of the analyzed sag deposits. A) Spherulitic rock intensely dolomitized (dark-blue) and partially silicified (yellow) with minor sphalerite (gray; indicated by red arrows) filling the matrix-dissolution porosity; B) Dolostone (dark-blue) partially silicified (yellow) with macrocrystalline calcite (light-blue) and Sr-barite (purple; indicated by orange arrows) partially filling vugular and fracture porosity; C) Coalescent crust of fascicular calcite and calcite spherulites (light-blue) partially dolomitized (dark-blue) and silicified (yellow); D) Intraclastic rudstone with incipient dolomitization (dark-blue) and strong silicification (yellow) preferentially affecting the interstitial spaces and edges of calcite intraclasts (light-blue); E) Chert with fractures and vugular pores filled by hydrothermal mineral phases: macroquartz (yellow), calcite (light-blue), Sr-barite (purple), and pyrite (brown); F) Sr-barite and celestine (purple) filling the fractures and replacing the pre-existing constituents in strongly brecciated, silicified and dolomitized argillaceous rock.

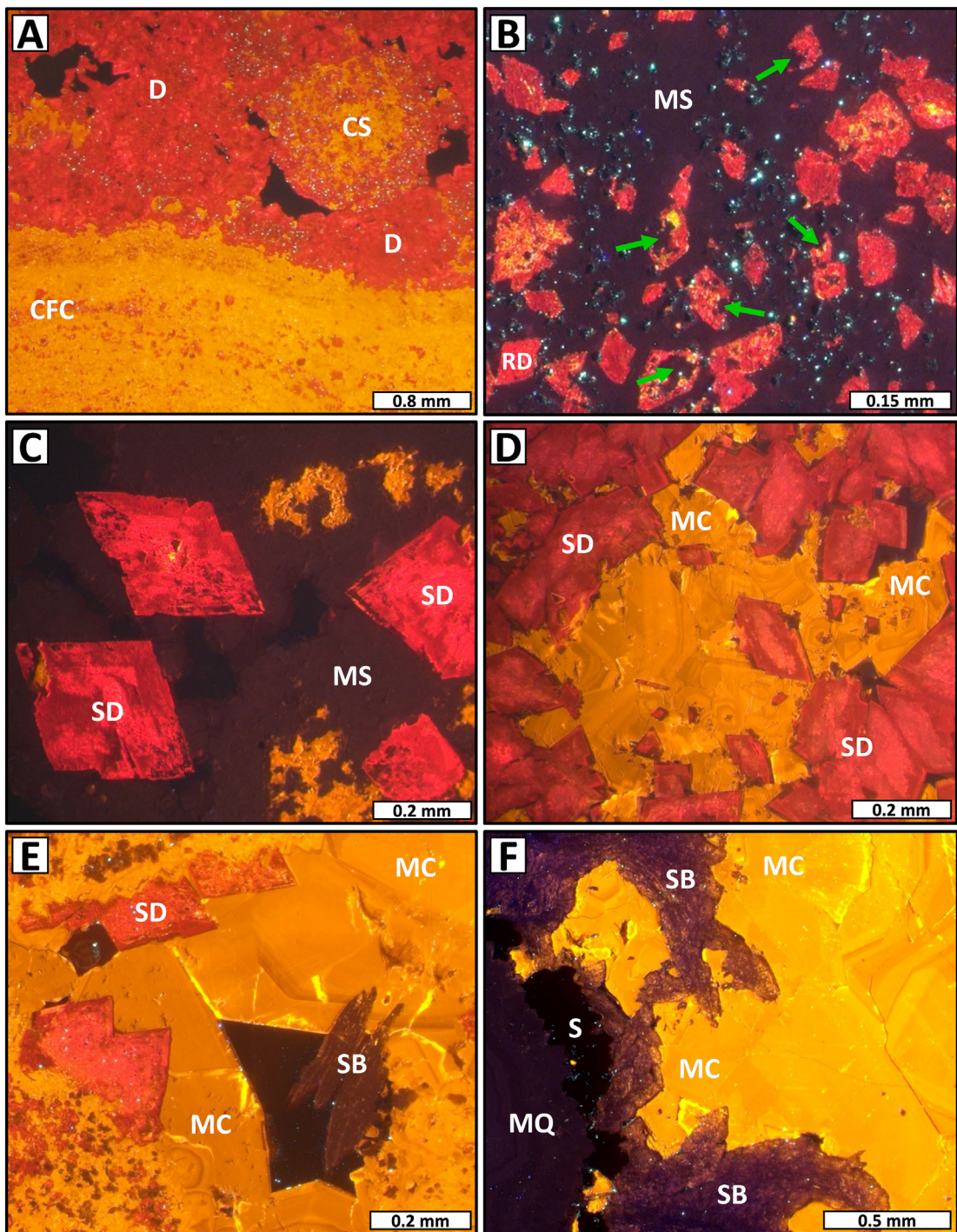


Fig. 11. Cathodoluminescence images of relevant aspects of the examined lithologic types and mineral phases. A) Partially dolomitized (D) coalescent crusts of fascicular calcite (CFC) and calcite spherulites (CS); B) Intensely silicified (black) and dolomitized (red) deposit with dolomite rhombs (RD), microcrystalline silica (MS) and svanbergite (light blue). Note the dolomite rhombs partially replaced by microcrystalline silica (green arrows); C) Complexly zoned saddle dolomite crystals (SD) partially surrounded and replaced by microcrystalline silica (MS); D) Zoned saddle dolomite (SD) and mosaic calcite (MC) filling vugular porosity; E) Sr-barite (SB), and zoned saddle dolomite (SD) and macrocrystalline mosaic calcite (MC) filling vugular porosity; F) Fracture in chert, completely filled with zoned macrocrystalline mosaic calcite (MC) and quartz (MQ), radiated Sr-barite (SB), and sulfides (S).

microcrystalline siliceous phases, moganite, tridymite, and cristobalite are associated with quartz and chalcedony, as verified in the XRD analyses. Crystal sizes within the cherts vary between 0.01 and 2.94 mm, with a mode of 0.11 mm. Microcrystalline and blocky dolomite is very common (Fig. 12B), replacing primary, syngenetic, and diagenetic constituents, such as Mg-clay deposits, intraclasts, and calcite crusts and spherulites, which commonly representing relicts from previous dolomitization.

Diagenetic phases replacing preexisting constituents in sag cherts include microcrystalline silica (Fig. 12A, B, C, E), micro to macrocrystalline quartz (Fig. 12D, E, F), fibrous and spherulitic chalcedony (Fig. 12B, C, E, F), mosaic calcite (Fig. 12D), and blocky and saddle dolomite (Fig. 12B, F). Subordinately, they were replaced by svanbergite, prismatic Sr-barite and celestine (Fig. 12D), fibro-radiated zeolite (Fig. 6D), and blocky sulfides (pyrite, chalcopyrite and galena) (Figs. 6E, F, 7F, 11F). Svanbergite is relatively common

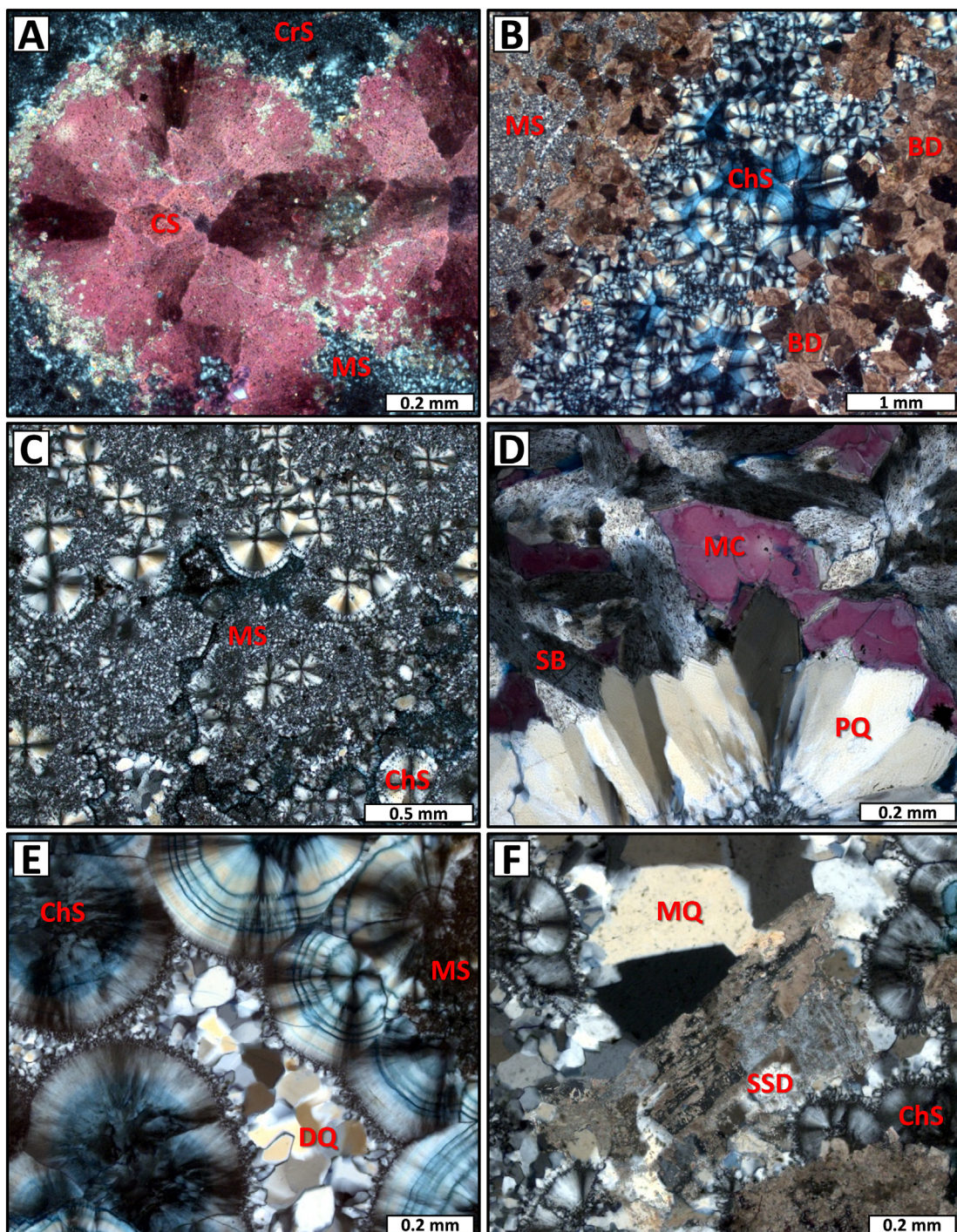


Fig. 12. Main aspects of diagenetic silica in cherts and partially silicified rocks. A) Calcite spherulites (CS) (stained red) partially replaced by microcrystalline (MS) and cryptocrystalline silica (CrS) (XP). Note that the silicification affected mostly the edges of the spherulites; B) Dolostone constituted by blocky dolomite (BD) partially replaced by microcrystalline silica (MS) and chalcedony spherulites (ChS) (XPL); C) Microcrystalline silica (MS) and chalcedony spherulites (ChS) totally replacing the preexisting constituents and cementing the vugular pores in chert (XP); D) Radial prismatic quartz (PQ), Sr-barite (SB) and macrocrystalline calcite (MC) filling vugular porosity (XP); E) Drusiform quartz (DQ) and spherulitic chalcedony (ChS) cementing vugular porosity in protolith totally replaced by microcrystalline silica (MS) (XP); F) Zoned saddle dolomite intensely silicified (SSD), macrocrystalline quartz (MQ), and spherulitic chalcedony (ChS) completely filling the vugular pore (XP).

and occurs as pseudocubic crystals varying from 1 to 100 μm (Fig. 5A), always disseminated in microcrystalline silica or within chalcedony spherulites, mainly where silicification affected clay-rich protoliths. WDS analyses of svanbergite yielded in average 19.4 mass% of SrO, 29.6% Al_2O_3 , 0.2% Ce_2O_3 , 0.1% CaO, 0.1% MgO, 0.1% La_2O_3 , 0.1% FeO, and 0.1% BaO.

Secondary pore types are mainly intercrystalline and intracrystalline aggregate. Intense fracturing and dissolution subsequent to silicification was responsible for an extensive, yet heterogeneous, formation of fracture and vugular porosity. Many vugs and fractures are partially to completely filled by microcrystalline silica; quartz as coarse mosaic, flamboyant and prismatic rims to drusiform; fibro-radiated and

spherulitic chalcedony; calcite as coarse mosaic; blocky and saddle dolomite; sulfates; sulfides; svanbergite; rutile; and bitumen (Table 2). Some fractures filled by prismatic quartz are often cut by others that are partially filled by macrocrystalline calcite (Fig. 10E).

Most of the observed silicification clearly occurred subsequent to dolomitization, as indicated by remnants of dolomitized constituents that are preserved within the silicified areas (Fig. 10). Some samples show pervasive silicification of dolomitized intraclasts and fascicular and spherulitic aggregates (Fig. 10C, D). At this stage, it is possible to identify only scarce remnants of dolomitized primary constituents (Fig. 10E). The syngenetic clay matrix remains were preferentially silicified in relation to the calcite spherulitic and fascicular aggregates. Quartz and chalcedony spherulites partially to fully replace preexisting constituents and fill growth framework, intra-crystalline aggregate, laminar, and vugular porosity. Commonly, dolomite rhombohedra with red CL present partial silicification along their edges (Fig. 11B). Small (2 to 20 μm) svanbergite crystals with light blue CL occur preferentially disseminated within microcrystalline quartz (Fig. 11B).

5. Discussion

5.1. Syngenetic Mg silicates

The occurrence of syngenetic magnesian clay minerals is reported in several alkaline and saline lakes (e.g., Bradley and Fahey, 1962; Tettenhorst and Moore, 1978; Darragi and Tardy, 1987; Calvo et al., 1999; Cuevas et al., 2003; Pozo and Galán, 2015). The predominant Mg layer silicates occurring in the Pre-Salt succession are kerolite, a hydrated form of talc, and mostly stevensite, which is a smectite (Bertani and Carozzi, 1985a, 1985b; Tosca and Wright, 2014; Sabato Ceraldi and Green, 2016).

The widespread precipitation of stevensite indicates that the Pre-Salt lacustrine environments of the Campos and Santos Basins presented high alkalinity ($\text{pH} \geq 10$), high concentrations of silica and magnesium, and low pCO_2 (Tosca and Masterson, 2014; Tosca and Wright, 2014, 2015). The commonly very fine and silky microfabric and the wavy laminations of these magnesian clay phases in the Aptian deposits (Fig. 3) suggest precipitation as a cryptocrystalline, with perhaps even a colloidal syngenetic phase, possibly as a poorly crystalline hydrated Mg-silicate gel (Tosca and Wright, 2014). The laminated stevensitic deposits were probably deposited in low-energy environments, while the ooids are likely to have been formed under some agitation caused by waves or currents, with peloids probably deposited in intermediate energy conditions (Armealenti et al., 2016; Herlinger Jr. et al., 2017). Fine-grained deposits of stevensite and other Mg silicates occur throughout the whole Aptian Pre-Salt succession, and their recurrent and widespread distribution indicates that they constituted the background of sedimentation in the wide, hyper-alkaline sag lakes. The salinity of the fluid is an important factor in Mg-clay precipitation (Pozo and Calvo, 2018).

The Mg-clay deposits were commonly dissolved, and/or replaced by silica, calcite, dolomite or magnesite. The widespread dissolution of Mg-clays in the Pre-Salt deposits probably occurred under eodiagenetic conditions related to the low stability and fast dissolution kinetics of stevensite in a scenario of high pCO_2 , with a pH below 8 (Tosca and Wright, 2015). The dissolution of stevensite and other Mg silicates may have occurred either by the influx of CO_2 related to magmatic and/or hydrothermal activity or by the dilution of lacustrine waters owing to relatively more humid climatic conditions (e.g., Renaut et al., 1986; De Wet et al., 2002).

5.2. Syngenetic and eodiagenetic calcite

The main Pre-Salt Aptian reservoirs commonly correspond to crusts made of coalescent aggregates of divergent fibrous fascicular-optic (sensu Kendall, 1977) calcite with predominantly vertical

and shrub-like growth, which are similar to abiotic stromatolites (Grotzinger and Knoll, 1999; Riding, 2008) and abiotic travertines (ray-crystal shrubs sensu Chafetz and Guidry, 1999) (Fig. 4A, B, C). According to Chafetz and Guidry (1999), the ray-crystal shrubs that are characteristic of some travertines, which are similar to those observed in the crusts of fascicular calcite of the sag deposits, are a product of chemical, abiotic precipitation related to CO_2 loss and evaporation. Likewise, Riding (2008) characterized the stromatolites formed by fibrous aggregates, such as those of the Pre-Salt interval, as a product of abiotic precipitation. These deposits could be identified as a coarse-crystalline, equant spar or radial-fibrous calcite.

The syngenetic magnesian clays deposits, with a subordinate amount of siliciclastic mud, constituted the substrate on and within calcite crusts and spherulites that were chemically precipitated (Fig. 13). The interruption and deformation of the stevensite laminations indicate that the Pre-Salt calcite spherulites were formed within these fine-grained deposits, replacing and displacing the clay laminations during eodiagenesis (Wright and Barnett, 2015) (Figs. 4E, F, 13B), and not, as suggested by Chafetz et al. (2018) “around bacterial colonies and/or their bioproducts, probably while afloat in a lacustrine water column before settling to the water-sediment interface”. The displacement is not linked to compaction, because the calcite spherulites between the stevensitic matrix laminations did not present features such as grain fracturing and/or deformation.

Therefore, the calcite spherulites were formed as concretions, replacing and/or displacing fine-grained deposits constituted by syngenetic magnesian silicates and minor extrabasinal siliciclastic mud (Fig. 13B). Larger and asymmetric spherulites formed closer to the water-sediment interface (WSI), and at a greater relative distance, smaller and symmetrical growth of spherulites took place. The distinction between spherulitic and fascicular growth forms was probably defined by the higher ionic supply and rate of precipitation for the latter, as well as by the availability of free space for vertical growth (Grotzinger and Knoll, 1999; Wright and Barnett, 2014; Wright and Tosca, 2016).

The fascicular calcite crusts are syngenetic precipitates that formed directly on the WSI (Fig. 13C, D). Their irregular stratification is related to the intercalation of levels of crystalline calcite with a finer texture, or mostly of fine-grained syngenetic Mg silicates and terrigenous sediments. The continuous fibrous crystalline fabric of the fascicular crusts characteristic of the main reservoirs of the Aptian Pre-Salt succession has been interpreted in Archean and Paleoproterozoic stromatolites (Grotzinger and Knoll, 1999; Riding, 2008) and in travertines (Chafetz and Guidry, 1999) as being a product of chemical, abiotic precipitation (Wright and Barnett, 2015; Herlinger Jr. et al., 2017). This interpretation differs from the processes of mineralization, encrustation or sediment trapping and binding by benthic microbial communities (Burne and Moore, 1987; Riding, 2000). Therefore, the name *microbialite* should not be used for those reservoirs.

The intense and extensive precipitation of thick and laterally coalescent fascicular calcite crusts was probably associated with changes in the lake water chemistry related to increased runoff during less arid periods, and/or with CO_2 input by magmatic and hydrothermal activity. The irregular stratification of the deposits was probably related to the interruption or decrease of calcite precipitation, thus promoting the intercalation with microcrystalline calcite aggregates or with fine-grained stevensitic or terrigenous mud deposits. The high frequency of these “cycles” throughout the succession would imply that the alternated precipitation of stevensite or calcite could not be promoted by large-scale changes in the chemistry of the huge sag lakes, but rather in local conditions, which are potentially related to patterns of circulation and/or stratification of the lake waters. The Mg-matrix is later dissolved and preserves only syngenetic and eodiagenetic constituents, fascicular calcite and spherulitic aggregates, and generates secondary porosity (Wright and Barnett, 2017; Herlinger Jr. et al., 2017).

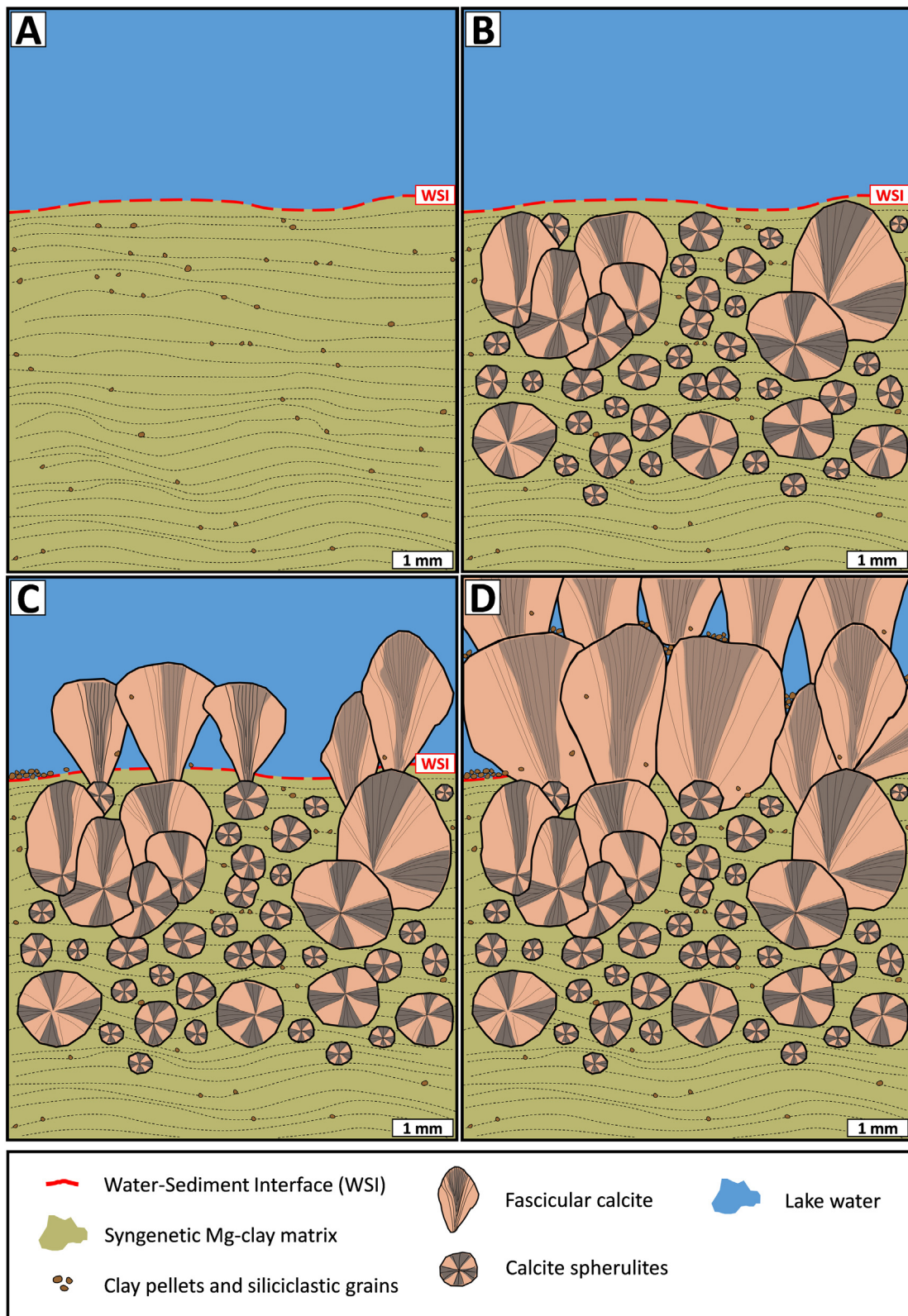


Fig. 13. Schematic representation of the genesis of typical Aptian Pre-salt deposits. A) Laminated deposits of syngenetic magnesian clays, with dispersed clay peloids and siliciclastic grains; B) Partial replacement and deformation of the Mg-clay matrix by calcite spherulites. Asymmetrical spherulites formed closer to the water-sediment interface (WSI); C) Non-coalesced fascicular aggregates of calcite precipitated on WSI with inter-aggregate growth-framework porosity. Clay peloids and siliciclastic grains included in some fascicular aggregates; D) Characteristic "cycle" showing the syngenetic crust of coalesced fascicular calcite aggregates at the top, and syngenetic Mg-clay matrix partially replaced and displaced by calcite spherulites in the middle and preserved at the base.

5.3. Diagenetic and/or hydrothermal processes and products

According to [Machel and Lonnee \(2002\)](#), the term hydrothermal dolomite is confusing and difficult to apply. Hydrothermal convection

that is capable of producing a pervasive dolomitization on a regional scale would be hydrologically impossible. For these same authors, it is possible to verify the existence of dolomitic deposits that are associated with hydrothermal activity related to faulting. The focused flow of

hydrothermal fluids through fault zones and/or unconformities could locally modify the reservoir quality (Jones and Xiao, 2013). However, the distinction of a hydrothermal mineral would only be possible if one considers its temperature of formation relative to the temperature of the surrounding rocks at the time of mineral formation.

The characteristics that are most commonly cited in the literature to define hydrothermal alteration in carbonate deposits are fluid temperatures higher than those of the host rocks; fluids directly or indirectly related to magmatic processes, with or without the introduction of juvenile water; fluid flow carried through fault and fracture systems; and local precipitation of "exotic" mineral assemblages with diverse compositions relative to the host rocks. However, it should be noted that several of these are not exclusive and that the characteristics mentioned above may be impractical to apply, such as a measurement of temperature higher than that of the host rocks. The processes of physicochemical alteration have certain determinant factors, such as the pH, temperature, and the composition of fluids that are rich in gases and ions.

Davies and Smith (2006) defined hydrothermal dolomitization as a process that occurs along structural lineaments under burial conditions, commonly at shallow depths, and that is related to hypersaline fluids with temperatures and pressures higher than those occurring in the host carbonate formation. According to Packard et al. (2001), some types of dolomite occurring in the Wabamun Group (Upper Devonian) in Parkland Field, Canada, exhibit a wide variety of crystallinity and microfabrics and are interpreted as products of hydrothermal dolomitization. Saddle dolomite occurs both as replacement for the original carbonate rock as well as by cement filling the secondary porosity. Dolomite deposits would be the result of recrystallization under the strong influence of successive fluids and formed during relatively short periods of intense hydrothermal activity. The porosity and permeability in host carbonate facies control the lateral extension of peripheral flow. Thus, the distribution and geometry of depositional and eodiagenetic facies of the host carbonates are critical for the lateral extension of hydrothermal dolomitization, as well as for the types, volume, and distribution of porosity (Xu et al., 2015).

Many of the Pre-Salt samples that were analyzed in the study area were strongly affected by fracturing, dissolution, recrystallization, pervasive dolomitization and silicification, and the precipitation of calcite, dolomite, quartz, chalcedony, Sr-barite, celestine, pyrite, chalcopyrite, galena, sphalerite, zeolite, and bitumen, mainly filling secondary porosity. This unusual mineral assembly is totally incompatible with the Pre-Salt carbonate host rock, which indicates that its precipitation occurred from hydrothermal fluids. Despite the relatively low-average percentages, hydrothermal phases are present in most rift and sag samples (Tables 1, 2). Both in lithologic types dolostones and cherts, as in intensely dolomitized and silicified samples, the mean values are slightly higher, which reveals their intrinsic relationship with hydrothermal dolomitization and silicification.

In many situations, recrystallization almost totally obscured the original fibrous fabric of the fascicular or spherulitic aggregates, which were transformed into a mosaic of anhedral calcite crystals. The partial replacement of the Mg-clay matrix, calcite spherulites, and fascicular aggregates by microcrystalline and blocky dolomite and magnesite is possibly the result of eodiagenetic and/or mesodiagenetic processes and occurs clearly prior to silicification (Figs. 4, 8, 10C, 11A, 14). Replacement of the Mg-clay by dolomite is a common feature and is quite clearly seen in the thin sections (Fig. 4D, E). A simplified reaction could be written as:



Such reaction would decrease the original very high pH. It occurs in both eodiagenetic and mesodiagenetic dolomitization but is more specific for processes that occurred during burial and under the influence

of hydrothermal fluids. Replacement of stevensite by finer-crystalline dolomite and by magnesite, as well as by microcrystalline quartz, has also occurred during eodiagenesis. The origin of the huge CO₂ volume required for the massive syngenetic and eodiagenetic precipitation of carbonates is one of many mysteries of the Pre-Salt section, but the coeval magmatism and probable mantle exhumation (e.g., Boillot et al., 1987; Manatschal and Bernoulli, 1999; Whitmarsh et al., 2001; Kusznir and Karner, 2007) can be considered the most likely sources.

The blocky dolomite does not present silica inclusions, which indicates that it is a pre-existing phase that was formed in the carbonate that was later silicified. The hydrothermal saddle dolomite in the rift and sag sections occurs both as replacement for the pre-existing constituents as well as cement filling primary and secondary porosity (Fig. 15). In many situations, these two types appear to have been formed contemporaneously from hot, hypersaline, and acidic fluids, favoring dissolution. When it occurs as a cement filling, the saddle dolomite is characterized by aggregates of large crystals with characteristic curved faces and undulating extinction, being more indicative of a hydrothermal configuration.

Important silicification has been described in sedimentary and volcanic rocks, as well as in pedogenetic and hydrothermal deposits, including occurrences as crusts, in individual layers, or even in whole packages in a disseminated pattern. Chert (sedimentary siliceous accumulations) may have many origins and be related to primary precipitation from siliceous gels (Shaw et al., 1990; Cough et al., 1996); diagenetic crystallization of diatoms (e.g., Kerrich et al., 2002); silicification of other sediments, notably carbonates (e.g., De Wet and Hubert, 1989; Teboul et al., 2019), radiolaria or sponge spicules; subaerial and subaqueous hydrothermal precipitation associated with hot spring systems (e.g., Renaut and Owen, 1988; Renaut et al., 2002); eodiagenetic modification of a precursor sodium silicate in saline and alkaline lakes (e.g., Sheppard and Gude, 1986); and subaerial precipitation of silcretes under arid climate and high alkalinity (pH higher than 9.0/9.5) (Hesse, 1989; Jiménez, 2011).

Silica sinters that formed in hot springs systems are characterized by a diversity of depositional environments that originate in a wide variety of fabrics, textures, and compositions and change laterally within the same system and between different occurrences. In these environments, high concentrations of dissolved silica, evaporation, rapid cooling, variations in the pH, cationic effects, physical hydrodynamics, and local conditions in the fluid escape area near hot springs produce siliceous sinters deposits of different geometries (e.g., Braunstein and Lowe, 2001; Gudry and Chafetz, 2003a, 2003b, 2003c; Jones and Renaut, 2003; Rodgers et al., 2004; Hinman and Walter, 2005; Jones et al., 2007; Campbell et al., 2015). The formation of superficial silica incrustations in sinters is frequently a product of the decrease in silica solubility with a temperature and/or pH drop, which is the main factor affecting the precipitation of hydrothermal silica. CO₂ degassing can lead to a sudden increase in pH, which increases the solubility of silica in the residual fluids (Jones and Renaut, 1996). Most lacustrine cherts are composed of microcrystalline and cryptocrystalline silica that precipitate in layers, nodules, and/or replacing other sediments.

Silicification in the Pre-Salt carbonates of the Campos Basin may be the result of synsedimentary, eodiagenetic and/or burial diagenetic processes, or the combination of all these. Several siliceous phases (e.g., chert, chalcedony, moganite, tridymite, cristobalite, and quartz) have been identified in the Pre-Salt lacustrine carbonate reservoirs. The silica in the studied area occurs as follows: relatively spaced syngenetic/eodiagenetic microquartz crusts with very low or no porosity (<3% of the described silica); diffuse and discontinuous hydrothermal chert lenses or masses composed of microquartz replacing the carbonate, with or without dolomitization (Figs. 14, 15); and microquartz, macroquartz, and chalcedony filling secondary pores and replacing saddle dolomite (Fig. 15).

The eodiagenetic chert crusts occur preferably near the top of the sag section and were formed possibly by the subaerial and subaqueous

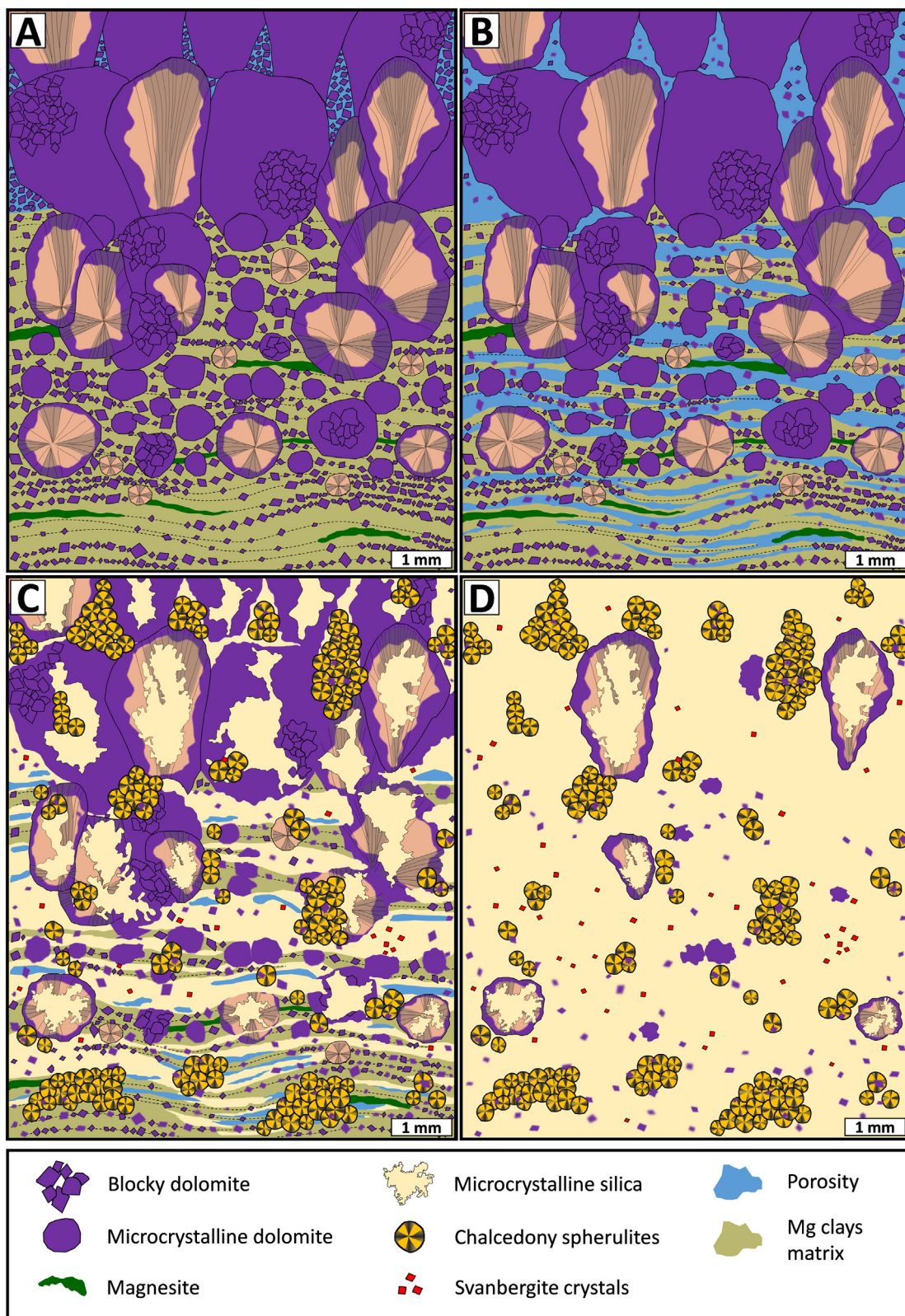


Fig. 14. Schematic representation of dolomitization, dissolution, and silicification in sag deposits. A) Dolomitization: microcrystalline and blocky dolomite partially replacing the Mg-clay matrix, calcite spherulites, and fascicular aggregates. Dolomite rhombohedra partially filling inter-aggregate pores. Magnesite pseudomorphically replacing some matrix laminations; B) Dissolution of the syngenetic Mg-clay matrix and part of the dolomitized calcite aggregates, thus generating laminar and vugular porosity; C) Silicification: microcrystalline quartz and chalcedony spherulites partially to fully replacing preexisting constituents, and filling growth framework, intra-crystalline aggregate, laminar, matrix-dissolution and vugular pores. Disseminated svanbergite crystals are selectively associated with microcrystalline silica; D) Selective internal silicification of some dolomitized fascicular and spherulitic aggregates. Scarce remnants of dolomitized primary constituents.

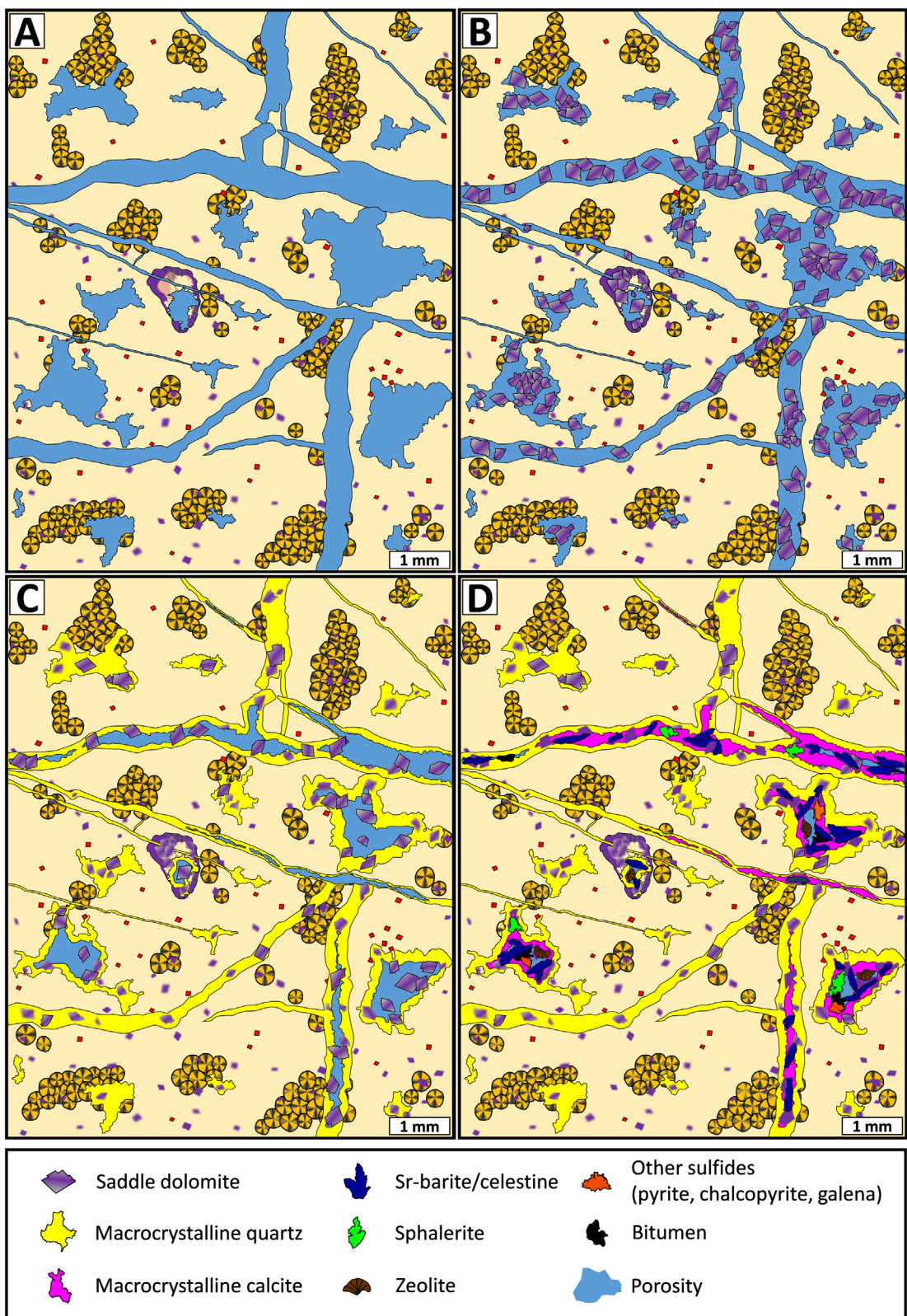


Fig. 15. Schematic representation of fracturing, dissolution, and hydrothermal phases filling secondary porosity. A) Fracturing and dissolution of pervasively silicified deposits, with the generation of fracture, channel, intra-crystalline aggregates, moldic and vugular pores; B) Saddle dolomite replacing preexisting constituents and mainly filling the secondary pores; C) Macrocrystalline, euhedral to subhedral quartz as prismatic rims and mosaics lining and filling the secondary pores and replacing saddle dolomite; D) Late phases: macrocrystalline calcite, radiated Sr-barite and celestine, fibro-radiated zeolite, euhedral to subhedral pyrite, chalcopyrite, galena and sphalerite, and massive bitumen filling the secondary pores.

hydrothermal precipitation associated with hot-spring systems or precipitation from evaporated meteoric fluids (Teboul et al., 2019). The pervasive hydrothermal replacement microquartz (chert) is

texturally distinct from eodiagenetic silica crusts that are concordant with depositional bedding. The replacement microquartz crystals occur in an equidimensional manner, suggesting that nucleation sites

were evenly distributed and that the supersaturation of the silica fluid was high (Gregg and Sibley, 1987). In many situations, it is possible to even notice the replacement of saddle dolomite by hydrothermal silica (Figs. 12F, 15C). Often, phases such as calcite, pyrite, chalcopyrite, galena, Sr-barite, celestine, sphalerite, svanbergite, zeolite, rutile, and bitumen, which are associated with siliceous phases, replace carbonates or cement primary and/or secondary pores (Fig. 15D).

In the Pre-Salt section, hydrothermal silicification occurs in carbonate packages associated with hydrothermal dolomites according to the model proposed by Packard et al. (2001). The hydrothermal fluids that are responsible for the dolomitization and silicification of carbonates would have had a common origin, only marginally evolved compared to the original composition. Saturated hydrothermal fluids with respect to silica, which are marginally saturated in relation to dolomite but are critically unsaturated with respect to calcite, were responsible for the selective substitution of preexisting carbonate with significant porosity creation. The characterization of the processes that are related to hydrothermal fluids is essential for the establishment of the most adequate production management strategy for these Pre-Salt reservoirs.

Analyzing the Pre-Salt interval in the Kwanza Basin, analogous to that of the Campos Basin, Poros et al. (2017) obtained fluid-inclusions homogenization temperatures (Th) between 95 and 115 °C in the dolomite cement, 95 and 125 °C in the silica (chert and chalcedony) replacing carbonate, and between 105 and 125 °C in the pore-filling mega-quartz. Those authors interpreted both the replacive chalcedony and the quartz cement that precipitated from high-T fluids ($T = 98\text{--}123\text{ }^{\circ}\text{C}$) associated with hydrocarbons (CH_4 and CO_2) in a burial diagenesis context. According to Girard and San Miguel (2017), temperatures ranging from 180 to 200 °C that were obtained from the fluid inclusions hosted in dolomite-calcite-quartz-filling intergranular and fracture pores and isotopic analyzes ($\delta^{18}\text{O}$, $\delta^{13}\text{C}$, $^{87}\text{Sr}/^{86}\text{Sr}$) on carbonates indicated a hydrothermal origin for the fluids responsible by the diagenesis that modified the Pre-Salt reservoirs in the Kwanza Basin. The analogy of the Kwanza Basin with patterns that were observed in the Campos Basin Pre-Salt supports the interpretation that the intense dolomitization, silicification and dissolution that were described in part of the analyzed samples may be related to the percolation of hydrothermal fluids through faults and hypogenic karst systems.

Some occurrences of APS minerals such as svanbergite are associated with hydrothermal mineralization related to magmatic and/or volcanic activity. According to Dill (2001), hypogenic APS mineralization can be formed from hydrothermal fluids at temperatures as high as 200 °C. Vila and Sillitoe (1991) described chalcedony, barite, and APS minerals that precipitated from hydrothermal fluids associated with Cu-Au porphyry-type and epithermal ore deposits in a magmatic-hydrothermal system. The formation of APS minerals is commonly associated with intrusion-driven hydrothermal systems, which may also be responsible for volcanic-hosted APS mineralization (Dill, 2001). In recent years, increasingly important diagenetic changes in carbonate reservoirs have been related to magmatic activities. Magmatic activities may not only provide hydrothermal fluids, but they also cause convection due to high temperature (Wilson et al., 2007; Xu et al., 2015). They may also result in the formation of fractures and secondary porosity, thus creating or modifying preferred paths for the migration and accumulation of hydrocarbons. According to Xu et al. (2015), in the Bachu region of the Tarim Basin, northwest of China, hydrothermal fluids migrated to Ordovician carbonate rocks along faults, fractures, unconformities and/or lithological contacts during the intrusive magmatism that occurred in the Cambrian and Permian. Hiemstra and Goldstein (2015) reported episodic injections of hydrothermal fluids associated with tectonic and magmatic activity on Pennsylvanian marine carbonates in the Indian Basin, U.S.A.

A potential source of Mg, silica and heat in hydrothermal systems in the Pre-Salt deposits of the Campos Basin could be provided by the intrusive and extrusive magmatic rocks that occur in the Campos Basin and/or by the serpentization of the exhumed mantle (Pinto et al., 2017). Winter et al. (2007) describe magmatic events occurring in the

rift phase during deposition of the sag section and in the Santonian/ Campanian. According to Wendte et al. (1998), the dolomitization that was caused by the brines that formed from the subsurface dissolution of evaporite deposits could have been discarded due to the low volumes of Mg.

5.4. Paragenetic evolution

The sequence of post-depositional processes affecting the sag and rift intervals was interpreted based on the paragenetic relationships of the processes and products with primary constituents, among each other and with the pores, as observed in optical, electronic, and cathodoluminescence images, and attributed to eodiagenetic, mesodiagenetic, and hydrothermal stages. The relative timing of each process/product, and its importance relative to porosity evolution are summarized in Fig. 16.

In the diagenetic evolution that was recognized in the analyzed Aptian rocks, fracturing occurred preferentially in the intervals that were more intensely affected by silicification. Dissolution promoted the generation of channel, intra-crystalline aggregates, moldic, and vugular pores (Fig. 15A). Zoned saddle dolomite with red-zonation CL patterns (Fig. 11C, D, E) occurs replacing pre-existing constituents and mainly filling secondary fracture, channel, growth framework, intra-crystalline aggregates, moldic, and vugular porosity (Fig. 15B). Prismatic rims and mosaic macrocrystalline quartz fills secondary pores, and replaces saddle dolomite (Fig. 15C). The late hydrothermal phases macrocrystalline calcite, zeolite, Sr-barite, celestine, pyrite, chalcopyrite, galena, sphalerite, and bitumen fill growth framework, fracture, and dissolution pores (Figs. 10, 11, 15). Sr-barite and celestine aggregates also occur replacing pre-existing constituents (Fig. 10E).

The paragenetic relationships among hydrothermal cements filling primary and secondary pores and/or replacing pre-existing constituents, indicate a predominance of the following precipitation sequence: saddle dolomite; quartz; pyrite, chalcopyrite, and galena; sphalerite; Sr-barite and celestine; macrocrystalline calcite; zeolite; and solid bitumen. Locally, the dissolution of some hydrothermal phases, such as saddle dolomite, sphalerite, zeolite, and Sr-barite, is responsible for the generation of intracrystalline porosity. Macrocrystalline mosaic calcite with orange-CL zonation commonly fills both primary and secondary porosity and occurs more frequently in large dissolution cavities and fractures (Fig. 11D, E, F).

Solid bitumen is described as a usual component in hydrothermal mineral paragenesis (e.g., Anderson, 1991; Mansurbeg et al., 2016) that is associated with relatively high-temperature barite, fluorite, sphalerite, and saddle dolomite. The occurrence of solid bitumen in barite hydrothermal mineralization is very common in some geological contexts (e.g., Paradis and Lavoie, 1996; Piqué et al., 2009). The dynamic and cyclical characters of the precipitation and dissolution processes of these mineral phases are related to intrinsic characteristics of hydrothermal alteration, associated with its transient, multiphase, and multi-episode aspects and to the variable chemical composition of the fluids. The mixing of hydrothermal and formation fluids may favor dissolution, especially in carbonate rocks, and the consequent formation of secondary porosity (Corbella et al., 2006; Biehl et al., 2016). Despite its possible reduced effect on the total pore volume, pores that connected more frankly and effectively in the vicinity of these hydrothermal vents should have a great influence on the dynamic behavior of the reservoir. In this system, the fractures acted as important conduits through which the hydrothermal fluids were injected, thus creating moldic and vugular porosity.

In the rift bioclastic deposits, much of the diagenesis occurred prior to compaction. During eodiagenesis, the following processes occurred: micritization; aragonite to calcite neomorphism; bioclasts dissolution; cementation by drusy/rims and blocky calcite and dolomite filling interparticle, intraparticle, moldic, and vugular porosity; and replacement of pre-existing constituents by microquartz and/or

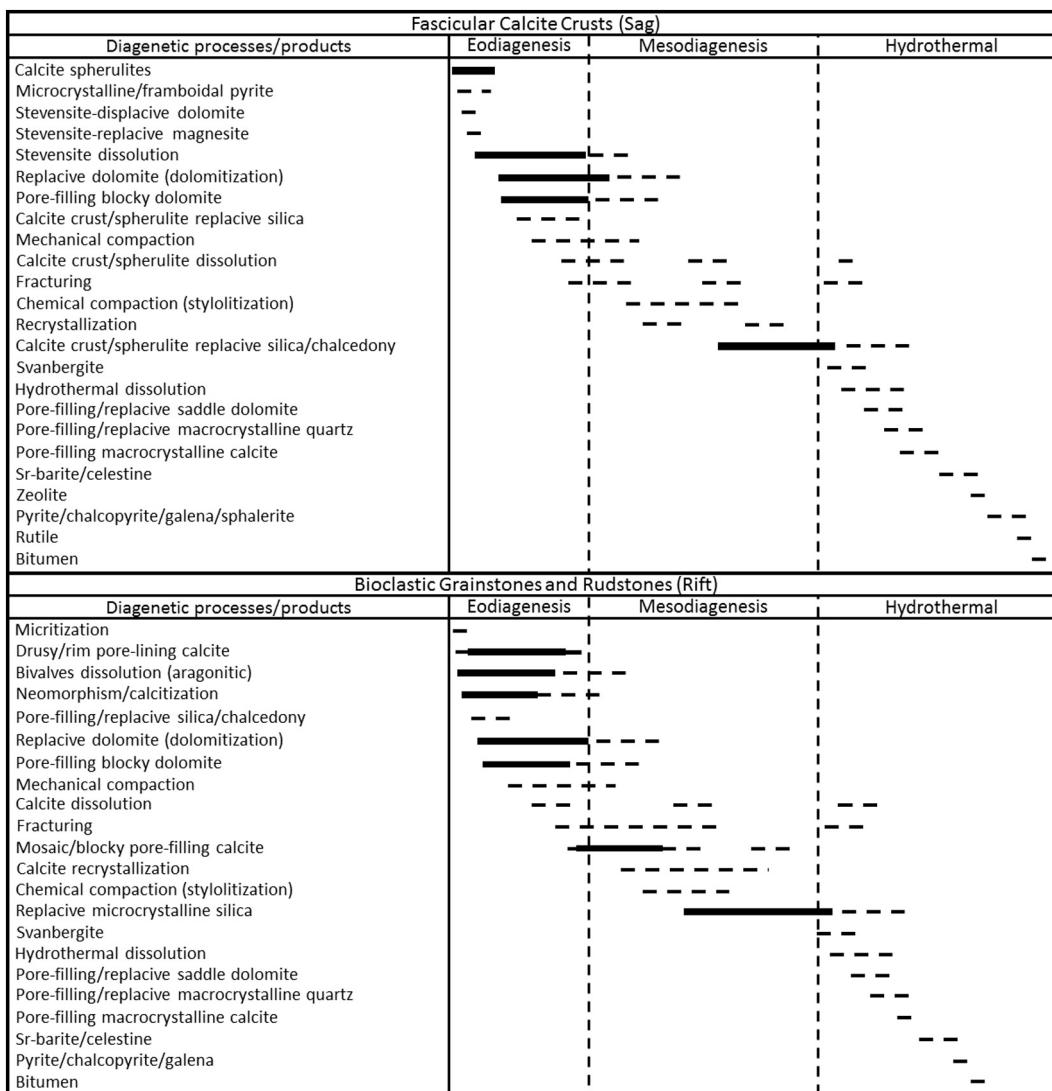


Fig. 16. Diagenetic sequences interpreted for sag fascicular calcite crusts and rift bioclastic grainstones and rudstones (modified from Herlinger Jr. et al., 2017). Thicker and dashed lines correspond to more and less intense processes and products, respectively.

chalcedony (silicification) and dolomite (dolomitization). The sequence of processes affecting these deposits during mesodiagenesis and hydrothermal alteration is very similar to that observed in the Aptian sag deposits, with the exception of zeolite and rutile, which were not observed in the analyzed rift samples. These mineral phases occur in very small quantities, and their absence in the rift samples is probably only a low sampling effect.

6. Conclusions

Syngenetic magnesian phyllosilicates (mostly stevensite, and kerolite), as clay laminations and peloids with subordinate siliciclastic mud contribution, constituted the background of the sag lacustrine sedimentation in the Pre-Salt carbonate reservoirs of the northern Campos Basin and the substrate onto which fascicular calcite crusts, and within which diagenetic calcite spherulites were precipitated. This variation promoted the formation of a cyclic pattern of laminated syngenetic magnesian clays at the base that were partially replaced and displaced by calcite spherulites in the middle, and syngenetic crusts of coalesced and non-coalesced fascicular calcite aggregates at the top.

The interruption and deformation of the stevensite laminations clearly indicates that the Pre-Salt calcite spherulites were formed within these fine-grained deposits during eodiagenesis, and not as particles in

the water column. The alternated precipitation of magnesian clay laminations and fascicular calcite crusts in the Aptian deposits of the northern Campos Basin was related to variations in pH, Mg, Si and Ca activities, temperature, and $p\text{CO}_2$ in the sag lacustrine waters. These changes in lake water chemistry occurred possibly due to magmatic events and/or a mantle contribution.

Porosity is predominantly secondary in the rift and sag intervals, where the main pore types are growth-framework, intercrystalline and intra-crystalline aggregates, interparticle, intraparticle, Mg-clay matrix dissolution, laminar, moldic, vugular, channel, fracture, and breccia. The most relevant cements filling primary, secondary dissolution, and fracture porosity in the rift and sag phases were calcite, dolomite, microcrystalline silica, chalcedony, quartz, pyrite, chalcopyrite, galena, Sr-barite, celestine, sphalerite, svanbergite, zeolite, rutile and bitumen. Many samples demonstrate dissolution, recrystallization, dolomitization and/or silicification, ranging from incipient to pervasive, locally originating dolostones and cherts. Typically, dolomite selectively replaced the interstitial Mg-clay sediments, while the calcite spherulitic and fascicular aggregates were only marginally dolomitized. Silicification commonly occurred subsequent to dolomitization.

Saddle dolomite, calcite, quartz, chalcedony, svanbergite, Sr-barite, celestine, pyrite, chalcopyrite, galena, sphalerite, zeolite, and bitumen were precipitated by the episodic flow of hydrothermal fluids, replacing

pre-existing constituents and filling fractures and dissolution porosity. Fault and fracture systems constituted important pathways through which fluid flow was focused, causing dissolution, precipitation of mineral phases, and reorganization of the pore systems. More limited hydrothermal processes were observed in the sag laminites and the in rift stevensitic ooidal arenites, possibly due to the limited primary porosity of these facies.

The hydrothermal alteration of the Pre-Salt deposits was probably related to magmatic activity or a mantle exhumation occurring in the Campos Basin during the Cretaceous. The importance of integrated studies for the characterization and prediction of depositional facies, diagenesis, hydrothermal alteration and, consequently, quality distribution in the Pre-Salt reservoirs should be emphasized.

Acknowledgements

We are grateful to Petróleo Brasileiro S.A., Petrobras, for permission to publish this paper and for supporting this study. We thank, specifically, the assistance provided by the Petrobras Research Center (CENPES) and the Regional Center for Technological Development and Innovation (CRTI) at the Federal University of Goias (UFG). The authors wish also to thank the editor and the reviewers for their constructive suggestions that helped improve the manuscript, and the Postgraduate Geosciences Program of the Rio Grande do Sul Federal University (UFRGS) for all their support and the use of their laboratories.

Appendix A. Supplementary data

Supplementary data to this article can be found online at <https://doi.org/10.1016/j.sedgeo.2019.01.006>.

References

- Abrahão, D., Warme, J.E., 1990. Lacustrine and associated deposits in a rifted continental margin – lower cretaceous Lagoa Feia Formation, Campos Basin, offshore Brazil. In: Katz, B.J. (Ed.), *Lacustrine Basin Exploration: Case Studies and Modern Analogs*. American Association of Petroleum Geologists, Memoir vol. 50, pp. 287–305.
- Alvarenga, R.S., Iacopini, D., Kuchle, J., Scherer, C.M.S., Goldberg, K., 2016. Seismic characteristics and distribution of hydrothermal vent complexes in the Cretaceous offshore rift section of the Campos Basin, offshore Brazil. *Marine and Petroleum Geology* 74, 12–25.
- Anderson, G.M., 1991. Organic maturation and ore precipitation in Southeast Missouri. *Economic Geology* 86 (5), 909–926.
- Armelenti, G., Goldberg, K., Kuchle, J., De Ros, L.F., 2016. Deposition, diagenesis and reservoir potential of non-carbonate sedimentary rocks from the rift section of Campos Basin, Brazil. *Petroleum Geoscience* 22 (3), 223–239.
- Austin, J.A., Uchupi, E., 1982. Continental-oceanic crustal transition off Southwest Africa. *American Association of Petroleum Geologists Bulletin* 66, 1328–1347.
- Baumgarten, C.S., Dultra, A.J.C., Scuta, M.S., Figueiredo, M.V.L., Sequeira, M.F.P.B., 1988. *Coquinas da Formação Lagoa Feia, Bacia de Campos: evolução da geologia de desenvolvimento*. Boletim de Geociências da Petrobras 2 (1), 27–36 (in Portuguese).
- Bertani, R.T., Carozzi, A.V., 1985a. Lagoa Feia Formation (Lower Cretaceous), Campos Basin, offshore Brazil: rift valley stage lacustrine carbonate reservoirs, I. *Journal of Petroleum Geology* 8, 37–58.
- Bertani, R.T., Carozzi, A.V., 1985b. Lagoa Feia Formation (Lower Cretaceous) Campos Basin, offshore Brazil: rift valley type lacustrine carbonate reservoirs, II. *Journal of Petroleum Geology* 8, 199–220.
- Biehl, B.C., Reuning, L., Schoenher, J., Lüders, V., Kukla, P.A., 2016. Impacts of hydrothermal dolomitization and thermochemical sulfate reduction on secondary porosity creation in deeply buried carbonates: a case study from the Lower Saxony Basin, Northwest Germany. *American Association of Petroleum Geologists Bulletin* 100 (4), 597–621.
- Boillot, G., Recq, M., Winterer, E.L., Meyer, A.W., Applegate, J., Baltuck, M., Bergen, J.A., Comas, M.C., Davies, T.A., Dunham, K., Evans, C.A., Girardeau, J., Goldberg, G., Haggerty, J., Jansa, L.F., Johnson, J.A., Kasahara, J., Loreau, J.P., Luna-Sierra, E., Moulade, M., Ogg, J., Sarti, M., Thurow, J., Williamson, M., 1987. Tectonic denudation of the upper mantle along passive margins: a model based on drilling results (ODP leg 103, western Galicia margin, Spain). *Tectonophysics* 132, 335–342.
- Bradley, W.H., Fahey, J.J., 1962. Occurrence of stevensite in the Green River Formation of Wyoming. *American Mineralogist* 47, 996–998.
- Braunstein, D., Lowe, D.R., 2001. Relationship between spring and geyser activity and the deposition and morphology of high temperature (>73 °C) siliceous sinter, Yellowstone National Park, Wyoming, USA. *Journal of Sedimentary Research* 71, 747–763.
- Burne, R.V., Moore, L.S., 1987. Microbialites: organosedimentary deposits of benthic microbial communities. *PALAIOS* 2, 255–262.
- Cainelli, C., Mohriak, W.U., 1999. Some remarks on the evolution of sedimentary basins along the Eastern Brazilian continental margin. *Episodes* 22, 206–216.
- Calvo, J.P., Blanc-Valleron, M.M., Rodríguez-Aranda, J.P., Rouchy, J.M., Sanz, M.E., 1999. Authigenic clay minerals in continental evaporitic environments. In: Thiry, M., Simon-Coinçon, R. (Eds.), *Palaeoweathering, Palaeosurfaces and Related Continental Deposits*. International Association of Sedimentologists, Special Publication vol. 27, pp. 129–151.
- Campbell, K.A., Guido, D.M., Gautret, P., Foucher, F., Ramboz, C., Westall, F., 2015. Geyserite in hot-spring siliceous sinter: Window on Earth's hottest terrestrial (paleo) environment and its extreme life. *Earth-Science Reviews* 148, 44–64.
- Carminatti, M., Dias, J.L., Wolff, B., 2009. From turbidites to carbonates: breaking paradigms in deep waters. *Offshore Technology Conference*. Houston, Texas, USA, OTC 20124.
- Carvalho, M.D., Praça, U.M., Silva-Telles, A.C., Jahnert, R.J., Dias, L.D., 2000. Bioclastic carbonate lacustrine facies models in the Campos Basin (Lower Cretaceous), Brazil. In: Gierlowski-Kordesch, E., Kelts, K.R. (Eds.), *Lake Basins through Space and Time. Studies in Geology* vol. 46. American Association of Petroleum Geologists, USA, pp. 245–255.
- Chafetz, H.S., Barth, J., Cook, M., Guo, X., Zhou, J., 2018. Origins of carbonate spherulites: implications for Brazilian Aptian Pre-Salt reservoir. *Sedimentary Geology* 365, 21–33.
- Chafetz, H.S., Butler, J.C., 1980. Petrology of recent caliche pisolithes, spherulites, and speleothem deposits from Central Texas. *Sedimentology* 27, 497–518.
- Chafetz, H.S., Guidry, S.A., 1999. Bacterial shrubs, crystal shrubs, and ray-crystal shrubs: bacterial vs. abiotic precipitation. *Sedimentary Geology* 126, 57–74.
- Choquette, P.W., Pray, L.C., 1970. Geologic nomenclature and classification of porosity in sedimentary carbonates. *American Association of Petroleum Geologists Bulletin* 54, 207–250.
- Chough, S.K., Kim, S.B., Chun, S.S., 1996. Sandstone/chert and laminated chert/black shale couplets, Cretaceous Uhangri Formation (Southwest Korea); depositional events in alkaline lake environments. *Sedimentary Geology* 104 (1), 227–242.
- Coniglio, M., Frizzell, R., Pratt, B.R., 2004. Reef-capping laminites in the Upper Silurian carbonate-to-evaporite transition, Michigan Basin, South-Western Ontario. *Sedimentology* 51, 653–668.
- Corbella, M., Ayora, C., Cardellach, E., Soler, A., 2006. Reactive transport modeling and hydrothermal karst genesis: the example of the Rocabruna barite deposit (Eastern Pyrenees). *Chemical Geology* 233, 113–125.
- Cuevas, J., De La Villa, R.V., Ramirez, S., Petit, S., Meunier, A., Leguey, S., 2003. Chemistry of Mg smectites in lacustrine sediments from the Vicalvaro Sepiolite Deposit, Madrid Neogene Basin (Spain). *Clays and Clay Minerals* 51 (4), 457–472.
- Darragi, F., Tardy, Y., 1987. Authigenic trioctahedral smectites controlling pH, alkalinity, silica and magnesium concentrations in alkaline lakes. *Chemical Geology* 63 (1–2), 59–72.
- Davies, G.R., 2004. Hydrothermal (thermobaric) dolomitization: rock fabrics and organic petrology. In: McAuley, R. (Ed.), *Dolomites – The Spectrum: Mechanisms, Models, Reservoir Development*. Canadian Society of Petroleum Geologists, Seminar and Core Conference, Calgary, Alberta, Canada, p. 17.
- Davies, G.R., Smith, L.B.J., 2006. Structurally controlled hydrothermal dolomite reservoir facies: an overview. *American Association of Petroleum Geologists Bulletin* 90 (11), 1641–1690.
- De Wet, B.C.C., Hubert, J.F., 1989. The Scots Bay Formation, Nova Scotia, Canada, a Jurassic carbonate lake with silica-rich hydrothermal springs. *Sedimentology* 36 (5), 857–873.
- De Wet, C.B., Mora, C.I., Gore, P.J.W., Gierlowski-Kordesch, E.H., Cuculo, S.J., 2002. Deposition and geochemistry of lacustrine and spring carbonates in Mesozoic rift basins, eastern North America. In: Renaut, R., Ashley, G. (Eds.), *Sedimentation in Continental Rifts*. SEPM, Special Publication vol. 73, pp. 309–325.
- Dias, J.L., 2005. Tectônica, estratigrafia e sedimentação no Andar Aptiano da margem leste brasileira. *Boletim de Geociências da Petrobras* 13, 7–25 (in Portuguese).
- Dias, J.L., Oliveira, J., Vieira, J., 1988. Sedimentological and stratigraphic analysis of the Lagoa Feia Formation, rift phase of Campos Basin, offshore Brazil. *Revista Brasileira de Geociências* 18, 252–260.
- Dickson, J.A.D., 1965. A modified staining technique for carbonates in thin section. *Nature* 205, 587.
- Dill, H.G., 2001. The geology of aluminum phosphate and sulphates of the alunite group minerals: a review. *Earth-Science Reviews* 53, 35–93.
- Girard, J.P., San Miguel, G., 2017. Evidence of high temperature hydrothermal regimes in the Pre-Salt Series, Kwanza Basin, Offshore Angola. *American Association of Petroleum Geologists Annual Convention and Exhibition*. Houston, Texas, USA (Abstracts).
- Goldberg, K., Kuchle, J., Scherer, C., Alvarenga, R., Ene, P.L., Armelenti, G., De Ros, L.F., 2017. Re-sedimented deposits in the rift section of the Campos Basin. *Marine and Petroleum Geology* 80, 412–431.
- Gregg, J.M., Sibley, D.F., 1987. Classification of dolomite rock textures. *Journal of Sedimentary Petrology* 57 (6), 967–975.
- Grotzinger, J.P., Knoll, A.H., 1999. Stromatolites in Precambrian carbonates: evolutionary mileposts or environmental dipsticks? *Annual Review of Earth and Planetary Sciences* 27, 313–358.
- Guidry, S.A., Chafetz, H.S., 2003a. Anatomy of siliceous hot spring examples from Yellowstone National Park, Wyoming, USA. *Sedimentary Geology* 157, 71–106.
- Guidry, S.A., Chafetz, H.S., 2003b. Depositional facies and diagenetic alteration in a relict siliceous hot-spring accumulation: examples from Yellowstone National Park, USA. *Journal of Sedimentary Research* 73, 806–823.
- Guidry, S.A., Chafetz, H.S., 2003c. Siliceous shrubs in hot springs from Yellowstone National Park, Wyoming, USA. *Canadian Journal of Earth Sciences* 40, 1571–1583.

- Herlinger Jr., R., Zambonato, E.E., De Ros, L.F., 2017. Influence of diagenesis on the quality of lower cretaceous Pre-Salt lacustrine carbonate reservoirs from northern Campos Basin, offshore Brazil. *Journal of Sedimentary Research* 87, 1285–1313.
- Hesse, R., 1989. Silica diagenesis: origin of inorganic and replacement cherts. *Earth-Science Reviews* 26, 253–284.
- Hiemstra, E.J., Goldstein, R.H., 2015. Repeated injection of hydrothermal fluids into downdip carbonates: a diagenetic and stratigraphic mechanism for localization of reservoir porosity, Indian Basin Field, New Mexico, USA. In: Agar, S.M., Geiger, S. (Eds.), *Fundamental Controls on Fluid Flow in Carbonates: Current Workflows to Emerging Technologies*. Geological Society, London, Special Publications vol. 406, pp. 141–177.
- Hinman, N.W., Walter, M.R., 2005. Textural preservation in siliceous hot spring deposits during early diagenesis: examples from Yellowstone National Park and Nevada, USA. *Journal of Sedimentary Research* 75, 200–215.
- Hodgson, W.A., 1968. The diagenesis of spherulitic carbonate concretions and other rocks from Mangakahia Group sediments, Kaipara Harbour, New Zealand. *Journal of Sedimentary Research* 38 (4), 1254–1263.
- Jiménez, J.I.P., 2011. *Sedimentología, Silicificaciones y Otros Procesos Diagenéticos en las Unidades Intermedia y Superior del Mioceno de la Cuenca de Madrid (zonas NE, NW y W)*. (PhD Thesis). Universidad Complutense de Madrid, Facultad de Ciencias Geológicas, Departamento de Petrología y Geoquímica, p. 336 (in Spanish).
- Jones, B., De Ronde, C.E.J., Renaut, R.W., Owen, R.B., 2007. Siliceous sublacustrine spring deposits around hydrothermal vents in Lake Taupo, New Zealand. *Journal of the Geological Society of London* 164 (1), 227–242.
- Jones, B., Renaut, R.W., 1996. Influence of thermophilic bacteria on calcite and silica precipitation in hot springs with water temperatures above 90 °C: evidence from Kenya and New Zealand. *Canadian Journal of Earth Sciences* 33, 72–83.
- Jones, B., Renaut, R.W., 2003. Hot spring and geyser sinters: the integrated product of precipitation, replacement, and deposition. *Canadian Journal of Earth Sciences* 40, 1549–1569.
- Jones, G.D., Xiao, Y., 2013. Geothermal convection in South Atlantic subsalt lacustrine carbonates: developing diagenesis and reservoir quality predictive concepts with reactive transport models. *American Association of Petroleum Geologists Bulletin* 97 (8), 1249–1271.
- Kendall, A., 1977. Fascicular-optic calcite: a replacement of bundled acicular carbonate cements. *Journal of Sedimentary Petrology* 47, 1056–1062.
- Kerrick, R., Renaut, R.W., Bonli, T., 2002. Trace element composition of cherts from alkaline lakes in the East African Rift: a probe for ancient counterparts. *SEPM Special Publication* 73, 275–294.
- Kusznir, N.J., Karner, G.D., 2007. Continental lithospheric thinning and breakup in response to upwelling divergent mantle flow: application to the Woodlark, Newfoundland and Iberia margins. In: Karner, G.D., Manatschal, G., Pinheiro, L.M. (Eds.), *Imaging, Mapping and Modelling Continental Lithosphere Extension and Breakup*. Geological Society, London, Special Publications vol. 282, pp. 389–419.
- Lepley, S., Piccoli, L., Chitale, V., Kelley, I., Quest, M., 2017. The importance of understanding diagenesis for the development of Pre-Salt lacustrine carbonates. *American Association of Petroleum Geologists Annual Convention and Exhibition*. Houston, Texas, USA (Abstracts).
- Leyden, R., Asmus, H., Zembruski, S., Bryan, G., 1976. South Atlantic diapiric structures. *American Association of Petroleum Geologists Bulletin* 60 (2), 196–212.
- Machel, H.G., 2004. Concepts and models of dolomitization: a critical reappraisal. In: Braithwaite, C.J.R., Rizzi, G., Darke, G. (Eds.), *The Geometry and Petrogenesis of Dolomite Hydrocarbon Reservoirs*. Geological Society, London, Special Publications vol. 235, pp. 7–63.
- Machel, H.G., Lonnee, J., 2002. Hydrothermal dolomite: a product of poor definition and imagination. *Sedimentary Geology* 152, 163–171.
- Manatschal, G., Bernoulli, D., 1999. Architecture and tectonic evolution of nonvolcanic margins: present day Galicia and ancient Adria. *Tectonics* 18, 1099–1119.
- Mansurbeg, H., Morad, D., Othmana, R., Morad, S., Ceriani, A., Al-aasm, I., Kolo, K., Spirov, P., Proust, J.N., Preat, A., Koyi, H., 2016. Hydrothermal dolomitization of the Bekhme formation (Upper Cretaceous), Zagros Basin, Kurdistan Region of Iraq: Record of oil migration and degradation. *Sedimentary Geology* 341, 147–162.
- McKenzie, D., 1978. Some remarks on the development of sedimentary basins. *Earth and Planetary Science Letters* 40, 25–32.
- Mercedes-Martín, R., Brasier, A.T., Rogerson, M., Reijmer, J.J.G., Vonhof, H., Pedley, M., 2017. A depositional model for spherulitic carbonates associated with alkaline, volcanic lakes. *Marine and Petroleum Geology* 86, 168–191.
- Mercedes-Martín, R., Rogerson, M., Brasier, A.T., Vonhof, H.B., Prior, T.J., Fellows, S.M., Reijmer, J.J.G., Billing, I., Pedley, H.M., 2016. Growing spherulitic grains in saline, hyperalkaline lakes: experimental evaluation of the effects of Mg-clays and organic acids. *Sedimentary Geology* 335, 93–102.
- Mohriak, W., Nemcok, M., Enciso, G., 2008. South Atlantic divergent margin evolution: rift-border uplift and salt tectonics in the basins of SE Brazil. In: Pankhurst, R.J., Trouw, R.A.J., Brito Neves, B.B., De Wit, M.J. (Eds.), *West Gondwana: Pre-Cenozoic Correlations across the South Atlantic Region*. Geological Society, London, Special Publications vol. 294, pp. 365–398.
- Muniz, M.C., Bosence, D.W.J., 2015. Pre-Salt microbialites from the Campos Basin (offshore Brazil): image log facies, facies model and cyclicity in lacustrine carbonates. In: Bosence, D.W.J., Gibbons, K.A., LeHeron, D.P., Morgan, W.A., Pritchard, T., Vining, B.A. (Eds.), *Microbial Carbonates in Space and Time: Implications for Global Exploration and Production*. Geological Society, London, Special Publications vol. 418, pp. 221–242.
- Neilson, J.E., Oxtoby, N.H., 2008. The relationship between petroleum, exotic cements and reservoir quality in carbonates – a review. *Marine and Petroleum Geology* 25, 778–790.
- Nürnberg, D., Müller, R.D., 1991. The tectonic evolution of the South Atlantic from Late Jurassic to present. *Tectonophysics* 191, 27–53.
- Packard, J.J., Al-Aasm, I.S., Samson, I., Berger, Z., Davies, J., 2001. A Devonian hydrothermal chert reservoir: the 225 bcf Parkland field, British Columbia, Canada. *American Association of Petroleum Geologists Bulletin* 85 (1), 51–84.
- Paradis, S., Lavoie, D., 1996. Multiple-stage diagenetic alteration and fluid history of Ordovician carbonate-hosted barite mineralization, Southern Quebec Appalachians. *Sedimentary Geology* 107 (1–2), 121–139.
- Pinto, V.H.G., Manatschal, G., Karpoff, A.M., Ulrich, M., Viana, A.R., 2017. Seawater storage and element transfer associated with mantle serpentinization in magma-poor rifted margins: a quantitative approach. *Earth and Planetary Science Letters* 459, 227–237.
- Piqué, À., Sabaté, À.C., Disnar, J.R., Borràs, F.G., 2009. In situ thermochemical sulfate reduction during ore formation at the Itxaspe Zn-(Pb) MVT occurrence (Basque-Cantabrian basin, Northern Spain). *Geologica Acta* 7 (4), 431–449.
- Poros, Z., Jagniecki, E., Luczaj, J., Kenter, J., Gal, B., Correa, T.S., Ferreira, E., McFadden, K.A., Elfritz, A., Heumann, M., Johnston, M., Matt, V., 2017. Origin of silica in Pre-Salt carbonates, Kwanza Basin, Angola. *American Association of Petroleum Geologists Annual Convention and Exhibition*. Houston, Texas, USA.
- Pozo, M., Calvo, J.P., 2018. An overview of authigenic magnesian clays. *Minerals* 8 (520), 1–22.
- Magnesian Clays: Characterization, Origin and Applications. In: Pozo, M., Galán, E. (Eds.), *AIPEA Educational Series*. 2. AIPEA, Bari, Italy, p. 380.
- Rabinowitz, P.D., Labrecque, J., 1979. The Mesozoic South Atlantic Ocean and evolution of its continental margins. *Journal of Geophysical Research* 84, 5973–6002.
- Renaut, R.W., Jones, B., Tiercelin, J.J., Tarits, C., 2002. Sublacustrine precipitation of hydrothermal silica in rift lakes: evidence from Lake Baringo, Central Kenya Rift Valley. *Sedimentary Geology* 148, 235–257.
- Renaut, R.W., Owen, R.B., 1988. Opaline cherts associated with sublacustrine hydrothermal springs at Lake Bogoria, Kenya, Rift Valley. *Geology* 16, 699–702.
- Renaut, R.W., Tiercelin, J.J., Owen, R.B., 1986. Mineral precipitation and diagenesis in the sediments of the Lake Bogoria Basin, Kenya Rift Valley. In: Frostick, L. (Ed.), *Sedimentation in the African Rift*. Geological Society, London, Special Publications vol. 25, pp. 159–175.
- Riding, R., 2000. Microbial carbonates: the geological record of calcified bacterial-algal mats and biofilms. *Sedimentology* 47 (Suppl. 1), 179–214.
- Riding, R., 2008. Abiogenic, microbial and hybrid authigenic carbonate crusts: components of Precambrian stromatolites. *Geologica Croatica* 61, 73–103.
- Rodgers, K.A., Browne, P.R.L., Buddle, T.F., Cook, K.L., Greatrex, R.A., Hampton, W.A., Herdianita, N.R., Holland, G.R., Lynne, B.Y., Martin, R., Newton, Z., Pastars, D., Sannazaro, K.L., Teece, C.I.A., 2004. Silica phases in sinters and residues from geothermal fields of New Zealand. *Earth-Science Reviews* 66, 1–61.
- Sabato Ceraldi, T., Green, D., 2016. Evolution of the South Atlantic lacustrine deposits in response to Early Cretaceous rifting, subsidence and lake hydrology. In: Sabato Ceraldi, R.A., Hodgkinson, T., Backe, G. (Eds.), *Petroleum Geoscience of the West Africa Margin*. Geological Society, London, Special Publications vol. 438, pp. 77–98.
- Saller, A., Rushton, S., Buambua, L., Inman, K., Mcneil, R., Dickson, J.A.D., 2016. Pre-Salt stratigraphy and depositional systems in the Kwanza Basin, offshore Angola. *American Association of Petroleum Geologists Bulletin* 100, 1135–1164.
- Schroeder, J.H., 1972. Fabrics and sequences of submarine carbonate cements in Holocene Bermuda cup reefs. *Geologische Rundschau* 61, 708–730.
- Shaw, P.A., Cooke, H.J., Perry, C.C., 1990. Microbialitic silcretes in highly alkaline environments: some observations from Sua Pan, Botswana. *South African Journal of Geology* 93 (5–6), 803–808.
- Sheppard, R.A., Gude, A.J., 1986. Magadi-type chert – a distinctive diagenetic variety from lacustrine deposits. In: Mumpton, F.A. (Ed.) *Studies in Diagenesis*. U.S. Geological Survey Bulletin vol. 1578, pp. 335–345.
- Teboul, P.A., Durlet, C., Girard, J.P., Dubois, L., Miguel, G.S., Virgone, A., Gaucher, E.C., Camoin, G., 2019. Diversity and origin of quartz cements in continental carbonates: example from the Lower Cretaceous rift deposits of the South Atlantic margin. *Applied Geochemistry* 100, 22–41.
- Teboul, P.A., Kluska, J.M., Marty, N.C.M., Debure, M., Durlet, C., Virgone, A., Gaucher, E.C., 2017. Volcanic rock alterations of the Kwanza Basin, offshore Angola – Insights from an integrated petrological, geochemical and numerical approach. *Marine and Petroleum Geology* 80, 394–411.
- Tettenhorst, R., Moore, C.E.J., 1978. Stevensite oolites from the Green River Formation of Central Utah. *Journal of Sedimentary Petrology* 48 (2), 587–594.
- Thompson, D.L., Stilwell, J., Hall, M., 2015. Lacustrine carbonate reservoirs from Early Cretaceous rift lakes of Western Gondwana: Pre-Salt coquinas of Brazil and West Africa. *Gondwana Research* 28, 26–51.
- Torsvik, T.H., Rousse, S., Labails, C., Smethurst, M.A., 2009. A new scheme for the opening of the South Atlantic Ocean and the dissection of an Aptian salt basin. *Geophysical Journal International* 177, 1315–1333.
- Tosca, N.J., Masterson, A.L., 2014. Chemical controls on incipient Mg-silicate crystallization at 25 °C: implications for early and late diagenesis. *Clay Minerals* 49, 165–194.
- Tosca, N.J., Wright, V.P., 2014. The formation and diagenesis of Mg-clay minerals in lacustrine carbonate reservoirs. *American Association of Petroleum Geologists Annual Convention and Exhibition*. Houston, Texas, USA (Search and Discovery Article #51002).
- Tosca, N.J., Wright, V.P., 2015. Diagenetic pathways linked to labile Mg-clays in lacustrine carbonate reservoirs: a model for the origin of secondary porosity in the Cretaceous Pre-Salt Barra Velha Formation, offshore Brazil. In: Armitage, P.J., Butcher, A.R., Churchill, J.M., Csoma, A.E., Hollis, C., Lander, R.H., Omma, J.E., Worden, R.H. (Eds.), *Reservoir Quality of Clastic and Carbonate Rocks: Analysis, Modelling and Prediction*. Geological Society, London, Special Publications vol. 435, pp. 33–46.
- Turner, S., Regelous, M., Kelley, S., Hawkesworth, C., Mantovani, M., 1994. Magmatism and continental break-up in the South Atlantic: high precision ^{40}Ar – ^{39}Ar geochronology. *Earth and Planetary Science Letters* 121, 333–348.

- Verrecchia, E.P., Freytet, P., Verrecchia, K.E., Dumont, J.L., 1995. Spherulites in calcareous laminar crusts: biogenic CaCO_3 precipitation as a major contributor to crust formation. *Journal of Sedimentary Research* 65A (4), 690–700.
- Vieira de Luca, P.H., Matias, H., Carballo, J., Sineva, D., Pimentel, G.A., Tritlla, J., Esteban, M., Loma, R., Alonso, J.L.A., Jiménez, R.P., Pontet, M., Martínez, P.B., Vega, V., 2017. Breaking barriers and paradigms in presalt exploration: The Pão de Açúcar discovery (offshore Brazil). In: Merrill, R.K., Sternbach, C.A. (Eds.), *Giant Fields of the Decade 2000–2010*. American Association of Petroleum Geologists, USA, Memoir vol. 113, pp. 177–194.
- Vila, T., Sillitoe, R.H., 1991. Gold-rich porphyry systems in the Maricunga Belt, northern Chile. *Economic Geology* 86, 1238–1260.
- Wendte, J., Qing, H., Dravis, J.J., Moore, S.L.O., Stasiuk, L.O., Ward, G., 1998. High-temperature saline (thermoflux) dolomitization of Devonian Swan Hills platform and bank carbonates, Wild River area, west-central Alberta. *Bulletin of Canadian Petroleum Geology* 46 (2), 210–265.
- White, N., McKenzie, D., 1988. Formation of the “steer’s head” geometry of sedimentary basins by differential stretching of the crust and mantle. *Geology* 16, 250–253.
- Whitmarsh, R.B., Manatschal, G., Minshull, T.A., 2001. Evolution of magma-poor continental margins from rifting to sea-floor spreading. *Nature* 413, 150–153.
- Wilson, M.I.J., Evans, M.J., Oxbury, N.H., Nas, D.S., Donnelly, T., Thirwall, M., 2007. Reservoir quality, textural evolution, and origin of fault-associated dolomites. *American Association of Petroleum Geologists Bulletin* 91, 1247–1272.
- Winter, W.R., Jahnert, R.J., França, A.B., 2007. Bacia de Campos. *Boletim de Geociências da Petrobras* 15, 511–529 (in Portuguese).
- Wright, V.P., Barnett, A., 2017. Classifying reservoir carbonates when the status quo simply does not work: a case study from the Cretaceous of the South Atlantic. *Search and Discovery Article #51419*. Adapted from oral presentation given at AAPG 2017 Annual Convention and Exhibition, Houston, Texas, USA, April 2–5, 2017.
- Wright, V.P., Barnett, A.J., 2014. Cyclicality and carbonate-silicate gel interactions in Cretaceous alkaline lakes. *American Association of Petroleum Geologists Annual Convention and Exhibition*, Houston, Texas, USA.
- Wright, V.P., Barnett, A.J., 2015. An abiotic model for the development of textures in some South Atlantic Early Cretaceous lacustrine carbonates. In: Grotzinger, J.P., James, N. (Eds.), *Microbial Carbonates in Space and Time: Implications for Global Exploration and Production*. Geological Society, London, Special Publication vol. 418, pp. 209–219.
- Wright, V.P., Tosca, N.J., 2016. Geochemical model for the formation of the Pre-Salt reservoirs, Santos Basin, Brazil: implications for understanding reservoir distribution. *Search and Discovery Article #51304*. Adapted from oral presentation given at AAPG Annual Convention & Exhibition, Calgary, Alberta, Canada, June 19–22, 2016.
- Xu, K., Yu, B., Gong, H., Ruan, Z., Pan, Y., Ren, Y., 2015. Carbonate reservoirs modified by magmatic intrusions in the Bachu area, Tarim Basin, NW China. *Geoscience Frontiers* 6, 779–790.
- Young, R.A., 1995. *The Rietveld Method*. International Union of Crystallography, Oxford University Press, Oxford, New York, NY, p. 298.